New methods and advances of high-resolution spectroscopy

I. L. Fabelinskiĭ and I. L. Chistyĭ

P. N. Lebedev Physics Institute, USSR Academy of Sciences
Usp. Fiz. Nauk **119**, 487–524 (July 1976)

We present the theoretical foundations of the method of using multipass Fabry-Perot interferometers and an iodine light filter to get high-contrast spectra. Plane Fabry-Perot interferometers are considered with two, three, or five successive passes of the light through them, as well as one- and two-pass spherical Fabry-Perot interferometers, and also their tandem combinations. Examples are given of experimental studies of molecular light-scattering spectra in phase transitions in imperfect crystals and liquid crystals, pressed powders, opaque crystals, and also acoustic magnon spectra. The resultant contrast of the spectra was as large as 10^{12} when multipass and tandem interferometers were used, and 10^5 when an iodine light filter was used.

PACS numbers: 07.45.+r, 07.40.+a

CONTENTS

1. INTRODUCTION

Even before the advent of laser light sources, high-resolution spectroscopy had made many outstanding advances. They included the discovery and study of the hyperfine structure of spectral lines, shifts, splittings, and broadenings of spectral lines in magnetic and electric fields, the fine structure of the Rayleigh line, and many other studies.

People used as high-resolution spectroscopes the Michelson echelon, the Lummer-Gehrcke plate, and the Fabry-Perot interferometer and etalon.

The development of high-resolution spectroscopy and comparison of the different high-resolution spectroscopes showed that the Fabry-Perot interferometer or etalon having plane or spherical mirrors has many advantages, both in resolution, dispersion, light-gathering power, stable operation, and in simplicity of interpretation of the spectrum in terms of frequencies or wavelengths. The instrumental profile in the Fabry-Perot spectroscope is also well known. The advantages of the Fabry-Perot spectroscope have proved to be so substantial that is has now supplanted all the others, and it practically enjoys a monopoly. People have been able to eliminate some of its defects to a considerable extent, as will be discussed below. Hence all our discussions will concern the Fabry-Perot interferometer or etalon, while its new applications will refer to various problems of studying molecular light-scattering spectra. Yet, of course, the method itself of using the interferometer can be applied to the most varied spectral studies.

As for light-scattering spectroscopy, and in particular, molecular light-scattering spectra, the potentialities of the method were restricted up to 1960 by the characteristics of the spectral line of the exciting light, rather than by the spectroscope. As a rule, these lines were so broad that one couldn't measure the true width of Mandel'shtam-Brillouin components.[1] Even though the instrumental profile of the spectroscope was very narrow, one could measure only the displacement of the components from the exciting line, and thus determine the speed of ultrasound, though with low accuracy.[1]

Upon the advent of laser light sources having narrow and intense stimulated-emission lines, people could substantially increase the accuracy of determining the positions of displaced lines, and even more importantly, they could discover a new phenomenon, such as the fine structure of the tail of the Rayleigh line, whose discovery did not seem possible theretofore.[3] Laser light sources permitted people to develop methods of homodyning

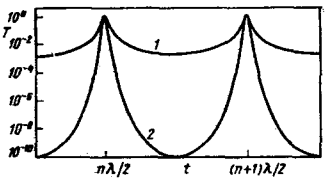

FIG. 1. The theoretical instrumental profile of the Fabry-Perot interferometer. A plane monochromatic wave is incident on the interferometer. T is the transmission of the interferometer, and t is the distance between the mirrors, The reflection coefficient of the mirrors is $R = 86\%$; the absorption in the mirror layer is $e = 0.2\%$; the mirror planes are fixed to an accuracy $\delta t = \lambda/100$.[12a] 1—Single passage of the light through the interferometer, 2—fivefold passage.

and heterodyning light and to make them practically accessible. These made it possible to study the shape of spectral lines no wider than several hertz.[4] Nowadays, when one uses the Fabry-Perot etalon for spectral measurements, the limit of resolution of close spectral lines of scattered light is determined, for example, not by the width of the exciting line (it can be very small in a single-frequency mode of operation of a laser), but by the width of the instrumental profile of the spectroscope. In turn, the latter is limited by the quality of the working of the surfaces of the mirrors in a plane interferometer, and by the departure from unity of the reflection coefficient of the mirrors in a spherical interferometer. There is a large set of physical problems for which the resolving power is quite sufficient to solve them, and sometimes even overly so, but contrast is lacking in the usual system of incorporating a Fabry-Perot etalon. The lack of contrast[1)] implies that one can't study or even detect weak satellites of spectral lines. These problems include all spectral studies of molecular light scattering in powders, liquid crystals, imperfect crystals, thin films, strongly-absorbing substances like silicon, germanium, and metals, and in all other cases in which a large amount of stray light at the unchanged frequency arises, e.g., narrow absorption lines and their fine structure, and many other problems.

Owing to the known form of the instrumental profile of the Fabry-Perot interferometer (Fig. 1), the large intensity of the stray light at the unshifted frequency causes a weak displaced line to be "swamped" in the intense "tail" of the instrumental profile. Hence it is not detected, owing to the low contrast of the spectral pattern.

Thus several important fields of spectral studies prove to lie outside the limiting possibilities of the usual methods of using high-resolution spectroscopes. Even long ago, the situation could be improved and the stray light could be suppressed to a considerable extent by setting a resonance filter in the path of the scattered and the stray light. One uses as the exciting light the resonance lines of mercury, sodium, or another element, and then sets a cuvette containing the vapor of the corresponding element in the path of the scattered light, and maintains a vapor density such as to absorb the light of the exciting line without attenuating the light at the displaced frequency.[5]

Iodine vapor is successfully used to absorb the exciting line $\lambda = 5145$ Å of argon-laser radiation.[6,7] We shall return again below to this latter method. Suppression of stray light by absorbing it in a light filter enhances the contrast of the spectral pattern, sometimes even by several orders of magnitude.

Another method of enhancing the contrast of the spectral pattern obtainable in the Fabry-Perot interferometer is based on passing the light beam through two interferometers of differing or like thicknesses that are arranged in succession. Houston[8] first applied this method as early as 1927. Houston also calculated the limiting resolution and contrast. Meissner then refined these calculations.[9] Later, Dufour[10] suggested passing the light being studied through the same filter twice. At the time that these first studies were being performed, interferometer mirrors were prepared by evaporating metals (silver or aluminum) having a high coefficient of reflection. Hence it made no sense to use more than two interferometers, owing to the great loss in light-gathering power of the apparatus. At the time of Dufour's studies, people were just beginning to use dielectric multilayer mirrors for which the absorption is much smaller, while the reflection is considerably greater than for metallic mirrors. People called instruments made of two successive Fabry-Perot etalons a "multiplex," "compound," or "tandem," but we can't say that any of these terms has supplanted the others.

The development of laser technology has stimulated the perfection of the preparation of dielectric mirrors having low light absorption, while the laser sources themselves have furnished experimenters with extremely intense and narrow spectral lines. All of this permitted Sandercock[11,12a] to use a Fabry-Perot interferometer through which he made the studied light beam pass several times. In his experiments with fivefold passage of the light through the interferometer, he attained a contrast $> 10^9$, whereas a single pass in this instrument gave a contrast of $\sim 10^2$ (see Fig. 1). A contrast of $\sim 10^{12}$ has subsequently been attained.[47] The fundamental way to increase the contrast by multiple passage through a Fabry-Perot etalon is simple, but one shouldn't think that the tecchnical realization of this method is also simple. We shall return again in the detailed description of the apparatus to the problem of the technical solution of this problem in working with a multipass interferometer.

The aim of this paper is to acquaint the reader with the methods of enhancing the contrast of an interference spectrum by using a multipass Fabry-Perot etalon and by using an iodine light filter, and also to report the fundamental physical results that have been obtained by using these methods.

Before we go on to describing the characteristics of the Fabry-Perot interference spectroscope having multiple passage of the light through it, we shall recall the fundamental characteristics of the plane and the spheri-

[1)] See Eq. (10) in Chap. 2 for the definition of contrast.

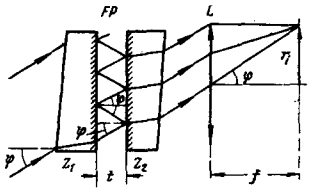

FIG. 2. Illustrating the calculation of the fundamental characteristics of a single-pass Fabry-Perot interferometer.[11] Z_1, Z_2 are the plates of the Fabry-Perot (FP) interferometer with the reflective layer of the inside. The distance between the plates is t; L is the objective in whose focal plane the interference pattern is observed; f is the focal length of this objective; r_1 is the radius of the ith interference ring, and φ is the angle of incidence of the ray on the interferometer.

cal Fabry-Perot etalons that are used in the ordinary system of single passage of the light through them.

2. FUNDAMENTAL CHARACTERISTICS OF THE PLANE FABRY-PEROT ETALON

Figure 2 shows a diagram of an apparatus having a Fabry-Perot etalon and the path of the rays in it. The conditions that describe the interference pattern are determined by the formula

$$2tn\cos\varphi = m\lambda. \tag{1}$$

Here, t, n, φ, m, and λ are the distance between the plane mirrors, the refractive index of the medium between the mirrors, the angle of incidence of the plane wave on the interference mirrors, the order of interference, and the wavelength of the light, respectively.

For a reflection coefficient $R<1$ of the mirrors, the intensity distribution in the interference spectrum is determined by the well-known Airy formula, which is here the "instrumental profile" of the interferometer. The Airy formula can be written in the following form for the case in which a parallel beam of monochromatic light falls on plane, identical interferometer mirrors, and its intensity is taken to be unity:

$$I(m)=\left(\frac{T}{1-R}\right)^2\frac{1}{1+(2F/\pi)^2\sin^2\pi m}. \tag{2}$$

Here R and T are the coefficients of reflection and transmission of the light for a single mirror of the interferometer, while for ideal plane mirrors,

$$F=F_R=\frac{\pi\sqrt{R}}{1-R}. \tag{3}$$

The quantity F is called the finesse.

If we let $m=m_0+\gamma$ in Eq. (2), where m_0 is an integer, while γ is the fractional part of the order, and further assume that $\pi\gamma$ is small, we can write Eq. (2) in the form

$$I(\gamma)=\left(\frac{T}{1-R}\right)^2\frac{1}{1+4F^2\gamma^2}. \tag{4}$$

Equation (4) implies that the total instrumental or apparatus half-width in fractions of the free spectral range (in fractions of the interference order) is

$$\frac{\delta\nu}{\Delta\nu}=2\gamma=F^{-1}. \tag{5}$$

Here the dispersion region, or free spectral range, of the plane Fabry-Perot interferometer is

$$\Delta\nu=\frac{1}{2t}\ (cm^{-1}),\qquad \Delta\lambda=\frac{\lambda^2}{2t}\ (\text{Å}). \tag{6}$$

The resolving power of this interferometer as a spectral apparatus is

$$A=\frac{\nu}{\delta\nu}=\frac{\nu F}{\Delta\nu}. \tag{7}$$

Equation (2) implies that the intensity will have a maximum for integral m, and it will be equal to

$$T_R=I_{\max}=\left(\frac{T}{1-R}\right)^2=\left(1-\frac{e}{1-R}\right)^2. \tag{8}$$

Here e is the absorption coefficient of the mirrors, and $e=1-R-T$. For half-integral m, the intensity will have the minimum:

$$I_{\min}=\left(\frac{T}{1+R}\right)^2. \tag{9}$$

By definition, the contrast of the interference pattern is

$$c=\frac{I_{\max}}{I_{\min}}=\left(\frac{1+R}{1-R}\right)^2\approx 1+\frac{4}{\pi^2}F^2. \tag{10}$$

The cited formulas imply that the finesse and the contrast are determined by the reflection coefficient R alone, while the apparatus half-width and the resolving power are still within the free spectral range of the etalon. If all this were true, then as $R\to 1$, we should expect that $c\to\infty$, $F\to\infty$, and $A\to\infty$, while $I_{\max}$ would differ from unity only because of light absorption in the mirrors of the interferometer.

The situation is actually much more complex. In the actual case, the Airy formula (2) does not describe all the substantial features of the interference pattern. The actual instrumental profile is far more complicated than the Airy formula, and it amounts to a convolution of at least three independent functions. These are the Airy function $I(\nu)$, which holds when $R<1$, other conditions being ideal; the function $S(\nu)$, which accounts for nonideal working of the plane surfaces of the mirrors, other conditions being ideal (the form of $S(\nu)$ depends on the form and nature of the distribution of inhomogeneities over the surface); and finally, the function $\Phi(\nu)$, which accounts for the finite entrance aperture of the radiation detector, also with other conditions being ideal. The nature of $\Phi(\nu)$ depends on the size and shape of the diaphragm at the detector input.

Consequently, the actual instrumental profile is a convolution of the functions $I(\nu)$, $S(\nu)$, and $\Phi(\nu)$. Here the half-width of this actual instrumental profile will be less than the simple sum of the half-widths of each separate function, but greater than each of the half-widths. All of these problems have been treated in detail in the re-

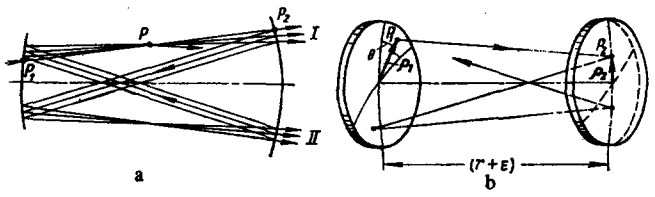

FIG. 3. Diagram of a spherical Fabry-Perot interferometer.[15] a) Path of the rays through the interferometer in the paraxial approximation; b) geometry of the rays inside the spherical Fabry-Perot interferometer. ρ_1 and ρ_2 are the distances from the axis of the interferometer to the entrance and exit points of the ray, and θ is the azimuthal angle between the radius-vectors of ρ_1 and ρ_2.

view by Jacquinot[13] and in the literature cited therein. Here it is essential only to stress that $\Phi(\nu)$ has a nature such that the finesse F_Φ arising from it can be made as great as one wishes, while the transmission T_Φ can be made very close to unity. Hence, for a plane etalon, we shall study in detail only $I(\nu)$ and $S(\nu)$.

The distributions $S(\nu)$ imposes the most substantial restrictions on the finesse and on all the associated characteristics of the interferometer. The finesse associated with the imperfect working of the plane surfaces can be expressed by the formula[13]

$$F_S=\frac{\lambda}{2\delta t}. \tag{11}$$

If the imperfect working of the surface is expressed in wavelengths, i.e., $\delta t=\lambda/m'$, then Eq. (11) is converted into

$$F_S=\frac{m'}{2}. \tag{12}$$

The actual finesse can never be greater than F_S; this is precisely why this quantity is often called the limiting finesse. The quantity F_S limits the instrumental half-width, the resolving power, and the contrast. The modern optical industry in individual cases reduces δt to $\lambda/200$, which gives $F_S=100$. However, as a rule, F_S in practice does not exceed 50, even in favorable cases.

The actual finesse F of a Fabry-Perot etalon is determined equally by the components F_R and F_S. When $F_R\approx F_S$, $F=0.7\,F_R$; when $F_S\gg F_R$, $F\to F_R$. The resultant finesse F is constituted as follows from the finesses F_i arising from the different factors:

$$F^{-2}=\sum_i F_i^{-2}. \tag{12a}$$

This implies that F will be governed by the smallest of the components.

In line with the roles of the three mentioned functions $I(\nu)$, $S(\nu)$, and $\Phi(\nu)$, the transmission of the etalon will be expressed as follows:

$$T_1=T_RT_ST_\Phi. \tag{13}$$

Here T_R is determined by Eq. (8), while T_S is determined by convoluting $I(\nu)$ with $S(\nu)$, and it would be equal to unity for ideal surfaces, but when $F_R=F_S$, $T_S=0.75$. T_Φ is determined by convoluting the three cited functions, and $T_\Phi=1$ for an infinitely narrow diaphragm. When the half-width $\Phi(\nu)$ equals the half-width of the convolution of $I(\nu)$ and $S(\nu)$, the transmission $T_\Phi=0.80$. Apparently, T_Φ is very close to unity in photoelectric recording, in which one uses very small apertures.

The foregoing and Eqs. (10) and (12) imply that the limiting contrast that one can get in the usual system of using a Fabry-Perot etalon will be

$$c=1+\frac{4}{\pi^2}\left(\frac{m'}{2}\right)^2. \tag{14}$$

This becomes inadequate in a number of cases, in particular those that we cited at the beginning. The free spectral range also often is inadequate. Hence the need arises of improving these characteristics.

3. THE FABRY-PEROT INTERFEROMETER WITH SPHERICAL MIRRORS

The Fabry-Perot interferometer with spherical mirrors (SFPI) was proposed by Connes,[14] and is now used as a high-resolution spectroscope.

The theory of this instrument has been developed in a series of studies.[15,20a] The SFPI is a resonator that consists of two spherical mirrors that are generally arranged confocally. In the confocal arrangement of the mirrors, the distance between them is twice the focal length of the mirrors. If a plane wave falls on the SFPI at some angle to the axis of the interferometer, then, as Fig. 3 shows, two groups of rays will exit from it, owing to the curvature of the mirrors of the interferometer (Fig. 3a shows the normals to the wavefronts). Group I will exit in the same direction as the incident ray. The rays of this group experience within the interferometer $4p$ reflections, where $p=0,1,2,\ldots$ Group II of rays will exit from the interferometer at some angle to the direction of the incident rays, while each ray undergoes $4p+2$ reflections. Interference occurs between the light waves in each group. Thus, two independent systems of interference rings arise, and one can see them in the focal plane of an objective placed after the SFPI.

Let the mirrors of the interferometer be arranged not exactly confocally, with a deviation fron confocality of $\varepsilon=t-r$, where t is the distance between the centers of the mirrors (Fig. 3b), while r is the radius of curvature of the mirrors. Then the path difference in wavelengths between the rays in each of the two groups will be

$$\tilde{m}=\tilde{m}_0-\tilde{m}', \tag{15}$$

where $m_0=(4/\lambda)(r+\varepsilon)$, and in the first approximation when $\rho/r\ll 1$,

$$\tilde{m}'=\left(\frac{\rho_1^2\rho_2^2}{r^3}\cos 2\theta+2\varepsilon\frac{\rho_1^2+\rho_2^2}{r^2}\right)\frac{1}{\lambda}; \tag{16}$$

here ρ_1 and ρ_2 are the distance between the axis of the interferometer and the entrance and exit points of the rays in the first and second mirrors, respectively, and

θ is the azimuthal angle (see Fig. 3b). If we consider only paraxial beams ($\theta \sim 0$ and $\rho_1 = \rho_2$), then we get from Eq. (16):

$$\tilde{m}' = \left(\frac{\rho^4}{r^3} + 4\varepsilon\,\frac{\rho^2}{r^2}\right)\frac{1}{\lambda}. \tag{17}$$

The intensity distribution in the interference pattern observed following the SFPI is analogous to Eq. (2). When the intensity of the incident light is taken to be unity, the intensity distribution for group I is determined by the expression

$$I = \left(\frac{T}{1-R^2}\right)^2 \frac{1}{1+(2\tilde{F}/\pi)^2 \sin^2 \pi\tilde{m}}, \tag{18}$$

and for group II,

$$I_2 = R^2 I_1, \tag{19}$$

where

$$\tilde{F} = \tilde{F}_R = \frac{\pi R}{1-R^2}. \tag{20}$$

Equations (18) and (19) imply that one will observe a maximum in the interference pattern when $\tilde{m}$ is an integer in the two cases of rays of group I and group II. If the light incident on the SFPI is well collimated, yet a small angle α remains between the axis of the light beam and the axis of the interferometer, then the two systems of fringes practically merge. Then their intensities add, and the intensity at the maximum will be

$$I_{\max} = (1+R^2)\left(\frac{T}{1-R^2}\right)^2 \approx \frac{1}{2}\left(\frac{T}{1-R}\right)^2 \quad (\text{when } R \sim 1). \tag{21}$$

Upon alignment[2)] of the SFPI with the input radiation incident on it, interference arises between the light waves of groups I and II. This leads to a twofold increase in the finesse $\tilde{F}$ and to the same increase in the transmission of the interferometer. In order to maintain such an alignment over a time period sufficient for an experiment, one must adopt special precautions.[15] The contrast, resolving power, and half-width of the instrumental profile will be determined by the same formulas (5), (11), and (10), but with F replaced by $\tilde{F}$. The free spectral range of the SFPI will be determined by two different expressions (with small corrections ignored). In a multimode regime of operation of the SFPI (lack of alignment),

$$\Delta\nu = \frac{1}{4t} \qquad (t = r + \varepsilon). \tag{22}$$

In the case of alignment and operation in the TEM_{00} mode,

$$\Delta\nu = \frac{1}{2t}. \tag{23}$$

In the SFPI, the quality of working of the mirror surfaces affects the finesse in exactly the same way as in the plane FPI. However, in the case of the SFPI, one can operate with very small regions of the surface of the mirrors, for which δt (see (11)) can easily be made considerably smaller than $\lambda/100$. Therefore $\tilde{F}_S$ can be far greater than $\tilde{F}_R$, even for reflection coefficients $R \approx 99\%$ (see (20)). The possibility of working with small surfaces (focusing the light into the interferometer) with the SFPI and the impossibility of working in this way with the plane FPI defines the substantial difference in the diffraction losses for the two types of interferometers. The finesses F_d and $\tilde{F}_d$ for plane and spherical resonators that arise from diffraction losses differ very greatly.[16] In fact, for a plane interferometer,

$$F_d = \frac{2\rho^2}{\lambda t}, \tag{24}$$

while for a spherical one,

$$\tilde{F}_d = 10^{5[(\rho^2/\lambda r)+1]}. \tag{25}$$

Here ρ is the radius of the working aperture of the interferometer. When $\rho = 0.05$ cm, $t = 5$ cm, and $\lambda = 5\times10^{-5}$ cm, we get $F_d = 20$, while $\tilde{F}_d = 10^{55}$. Hence, evidently, the diffraction losses for the SFPI have no effect on the finesse F nor on any of the quantities associated with it. The actual finesse F of the interferometer is made up from its components according to Eq. (12a).

For the SFPI, the smallest finesse value involves the departure of the reflection coefficient of the mirrors from unity. In order to avoid losing the great finesse in the SFPI, one must not diminish the light-gathering power of the instrument, and thus one must choose correctly the dimensions of the diaphragm of the radiation detector. If we choose the size of the diaphragm at the output of the SFPI to be

$$\rho_S = (r^3\lambda F^{-1})^{1/4}, \tag{26}$$

then the resolving power will decline by only 30%. Calculations show that, if the radius of the mirrors of the SFPI $r \geq D/5$, where D is the diameter of the plates of the plane Fabry-Perot interferometer, then the light-gathering power of the spherical Fabry-Perot interferometer is greater than for the plane interferometer. A detailed comparison of the light-gathering powers of the plane and spherical FPI has been made in[15].

4. THE TANDEM OR COMPOUND AND MULTIPASS FABRY-PEROT INTERFEROMETERS

One needs a large distance between the mirrors in order to get a high enough resolution of close-lying spectral lines. Then the free spectral range, or the free region between adjacent interference orders is small (see (6)), and superposition of lines of adjacent orders can arise. Hence we need to be able to attain a large enough free spectral range with substantial resolution.

This difficulty was overcome by Houston[8] and by Gercke and Lau,[17] who designed instruments having two Fabry-Perot etalons of differing thicknesses arranged in tandem. Figure 4 shows schematically two

[2)] Alignment is effected when $\alpha = 0$ and the phase surface of the wave coincides with the surface of the mirrors.

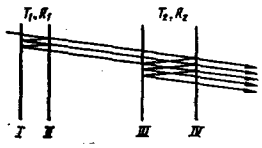

FIG. 4. Diagram of a tandam Fabry-Perot interferometer. The tandem combination consists of etalons of differing thickness and differing reflection and transmission coefficients of the mirrors.

etalons of differing thickness and differing effective coefficients of reflection and transmission. The results of the calculations that lead to Eqs. (27) and (28) (see below) hold if the path differences between the planes *I* and *III*; *I* and *IV*; *I* and *III*; and *II* and *IV* are greater than the coherence length of the light being emitted: $L=\lambda^2/\delta\lambda=\delta\nu^{-1}$ cm. For practically all cases of light-scattering spectra in gases, liquids, and solids at different temperatures (perhaps except for liquid-helium temperatures), the Mandel'shtam–Brillouin components have half-widths such that L is no greater than 5–150 cm. In these cases, the needed distance between the etalons is easily attained experimentally. Yet if we are dealing with light whose coherence length is very great, we should select the mutual distance between the etalons in a special way. This can lead to better results than in the case of light of small coherence length, though an incorrect choice of the mutual distance can lead to poorer results. However, we shall not discuss the case of large L here.

If the ratio of the thicknesses of the two etalons is integral, then the free spectral range in this instrument will be determined by that of the thin etalon, while the resolving power will prove to be somewhat larger than that of the thick etalon. It was shown in[9] that the resolving power of a tandem (compound) etalon made of two identical etalons will be 1.61 A, where A is the resolving power of one etalon. The calculation was done for the case in which one adopts the Rayleigh criterion for resolution of two close-lying spectral lines. The increase in finesse and resolving power in the compound etalon is not so large as the increase in contrast. According to the calculations of[9],

$$I(m_1;\ m_2)=\frac{T_1^2/(1-R_1)^2}{1+(2F_1/\pi)^2\sin^2\pi m_1}\,\frac{T_2^2/(1-R_2)^2}{1+(2F_2/\pi)^2\sin^2\pi m_2}. \tag{27}$$

Equation (27) implies that when the two etalons have the same thickness ($m_1=m_2=m$) and the same coefficients of reflection and transmission ($R_1=R_2=R$ and $T_1=T_2=T$), then

$$I(m)=\left(\frac{T}{1-R}\right)^4\left[\frac{1}{1+(2F/\pi)^2\sin^2\pi m}\right]^2. \tag{28}$$

In Eq. (27), we should take F_1, F_2, T_1, and T_2 to be the resulting values in the sense of Eqs. (12a) and (13). Equations (28) and (10) imply that the contrast in this case will be

$$c_2=c_1^2,$$

where c_1 is given by Eq. (10).

Dufour[10] has proposed using one etalon instead of two identical etalons lying in succession, but with the light made to pass through it twice. However, this suggestion did not receive the deserved attention, even after the advantages of this double-pass interferometer had been demonstrated experimentally.[16]

Intense laser light sources for exciting scattered light and low-absorption, multilayer dielectric interferometer mirrors have permitted people to apply the multipass Fabry-Perot etalon very effectively. This was shown in a series of excellent physical studies by Sandercock,[11,19] and it has subsequently been applied successfully by him and other physicists. These studies have achieved instruments with not only two passes of the light through the etalon, but also with a large number of passes. Figure 5 shows a diagram of one, two, three, and five passes of the light in a plane FPI. In order to characterize a multipass Fabry-Perot etalon, we should find expressions for the half-width of the interference fringes, determine its finesse, and the contrast and transmission of the etalon, i.e., find characteristics analogous to those of Eqs. (3), (5), and (8).

If we generalize Eq. (28) from two to n passes, and assume for simplicity, without restricting generality, that $I_{max}=1$, we can find the half-width of the interference fringes after n passes of the light through a given etalon from the condition

$$\left(\frac{1}{1+4F_1^2\gamma_n^2}\right)^n=\frac{1}{2}. \tag{29}$$

Hence we easily obtain that the half-width of the interference fringes in fractions of an interference order is

$$\frac{\delta\nu}{\Delta\nu}=2\gamma_n=(2^{1/n}-1)^{1/2}F_1^{-1}. \tag{30}$$

Upon comparing this expression with (5), we find that the resultant fineese is

$$F_n=F_1(2^{1/n}-1)^{-1/2}. \tag{31}$$

The contrast of the interference pattern after n passes will be

$$c_n=c_1^n=\left(1+\frac{4}{\pi^2}F_1^2\right)^n\approx\left(\frac{2}{\pi}F_1\right)^{2n}. \tag{32}$$

We can easily express in terms of F_n the half-width of the interference fringes and the resolving power of the

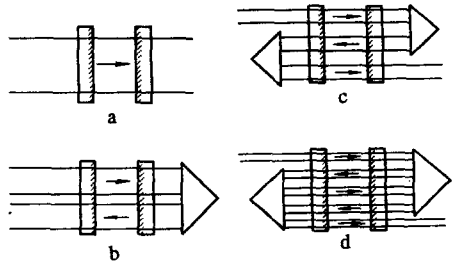

FIG. 5. Variants of Fabry-Perot etalons having varying numbers of passes. Triple prisms are used to return the rays. a) One pass, b) two, c) three, and d) five passes.

interference spectroscope.

Equations (29)–(32) imply that the contrast increases quite significantly with increasing number of passes of the light, with a relatively small increase in the finesse and the resolving power. Yet the intensity at the maximum of an interference fringe is determined by the quantity

$$T = (T_I T_S)^n. \tag{32a}$$

Sandercock's first exepriments[11] used a two-pass Fabry-Perot etalon.

If $c_1 \sim 10^2$–10^3 in a single-pass etalon, then in the same interferometer with two passes, $c_2 \sim 10^4$–10^6. This implies that satellites that amount in intensity to 10^{-3}–10^{-5} of the central line can be observed in the spectrum and studied with two passes.

If the light passes twice through the interferometer, then as we can easily obtain from (31), the finesse increases by a factor of 1.57. Sandercock's studies[12,19] used a fivefold passage of a beam through a given interferometer. Here the contrast attained values $c_n \approx 10^{10}$, while the finesse increased in comparison with a single pass by a factor of 2.56.

In the case of five passes, it is not expedient to use an interferometer having the same reflection coefficient as in the ordinary case, for which one chooses $F_R = F_S$ (then $F_1 = 0.7\, F_R$[13]). In the five-pass case, it is expedient to use $F \approx 40$. This gives quite good resolution for studying the fine structure of a molecular light-scattering line, it requires only $F_1 \sim 15$, and for $F_S = 3F_R$, it is satisfied for mirrors worked to an accuracy $\delta t = \lambda/100$. The low value of F_R means that T_I is large. For $F_R = 15$, we get from (3) that $R = 87\%$, and we get from Eq. (8) the value $(T_I)^5 \sim 90\%$. The transmission $(T_S)^5 \sim 80\%$, and thus we can expect a maximum transmission T of about 70% (see (32a)). Figure 1 shows a graph of the instrumental profile for $F_5 = 40.5$ in the cases of one and five passes.

5. THE TWO-PASS FABRY-PEROT INTERFEROMETER WITH SPHERICAL MIRRORS

In contrast to the above-studied multipass Fabry-Perot interferometer with plane mirrors, in which the rays of the successive passes are displaced with respect to one another, and they occupy different regions of the surface of the mirrors, the ray passes twice through the same region of the surface of the mirrors in the interferometer with spherical mirrors. In order spatially to separate the rays in opposite directions in the two-pass SFPI, one polarizes them orthogonally. The two-pass Fabry-Perot interferometer with spherical mirrors can have the same high contrast as the interferometer with plane mirrors, but it is more stable to external mechanical influences (less sensitive to misalignment of the mirrors due to mechanical vibrations), and it does not require automatic devices for maintaining the high degree of "parallelism" of the mirrors. Therefore this interferometer can be preferable in a number of cases. Figure 6 gives a diagram that explains the principle of operation of a two-pass SFPI. It has been developed and proposed by Cannell, Lunacek, and Dubin[20] for spectral studies requiring high contrast. As Fig. 6 shows, linearly polarized light is directed onto a Glan-Thompson prism that is arranged to transmit completely the light of the given polarization. Then this light passes through the interferometer and a quarter-wave plate cut from a uniaxial crystal. One orients the plate so that the optic axis of the crystal lying in the plane of the plate makes a 45° angle with the polarization direction of the incident light. The light is reflected backwards with a curved mirror, and it passes through the $\lambda/4$ plate a second time. Here the light changes its original linear polarization into the orthogonal direction. Upon passing through the Fabry-Perot interferometer, it is reflected from the diagonal plane of the Glan-Thompson prism, and it is brought outside by using an attached small prism. The small prism is cemented to the Glan-Thompson prism with Canada balsam in order to eliminate undesired reflections and light loss.

One uses in the system two aperture diaphragms A_1 and A_2, which restrict the diameter of the light beam on the spherical Fabry-Perot plates. In order that all the light that passes into the interferometer through the diaphragm A_1 should be returned back, the spherical mirror M having the radius of curvature R is set at the distance D from the diaphragm A_2, as determined by the relationship:

$$D = 0.5\,[(R - L) + \sqrt{(R - L)^2 + 2RL}]. \tag{33}$$

Under this condition, the diaphragm A_1 is completely imaged onto the diaphragm A_2, and vice versa. The quantity L amounts to the distance between the diaphragm A_2 and the image A_1' of the diaphragm as created by the mirror P_2. The dimensions of the diaphragms A_1 and A_2 are chosen to minimize the width of the instrumental profile of the interferometer. The condition $A_2 = A_1' D/(D + L)$ must be satisfied in order to eliminate light loss. Here the diameter of the image formed by the mirror M at the point A_1' will equal the diameter of the image at the point A_2. Then the contrast of the interference pattern increases practically according to the same law as in the plane FPI.

In the described system (see Fig. 6), the possible stresses within the glass plates of the interferometer will give rise to birefringence, whereby the contrast of the spectral pattern will be lowered. Therefore the

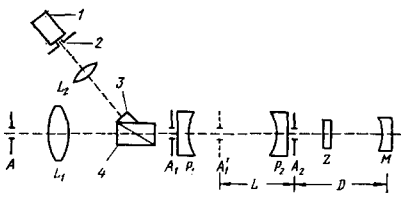

FIG. 6. Diagram of the arrangement of optical parts in a two-pass SFPI.[20] 1—radiation detector, 2—point aperture, 3—attached prism, 4—Glan-Thompson prism, A—entrance aperture, L_1—collimating lens, A_1—intermediate aperture, A_2—exit aperture, P_1 and P_2—interferometer mirrors, Z—quarter-wave plate, M—reflecting mirror, and L_2—focusing lens.

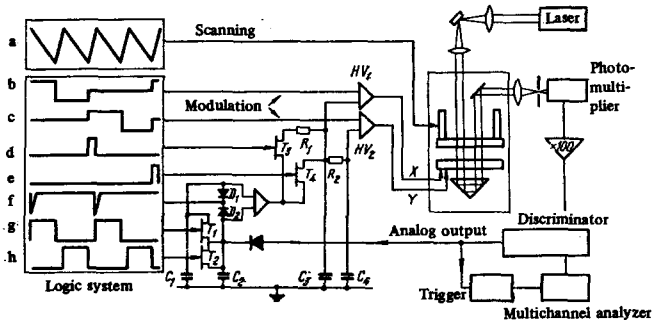

FIG. 7. Diagram of a two-pass plane Fabry-Perot interferometer, together with the system for scanning, maintenance of parallel mirrors, and recording the spectrum (see text).[11]

glasses for this interferometer must be chosen with especial care.

It is hard to effect more than two passes in the SFPI, yet if it turns out that the contrast in two passes does not suffice, then one can resort to a sequential arrangement of two or several SFPI's, analogously to what was done in[21].

6. ESTABLISHING AND MAINTAINING THE PARALLELISM OF THE MIRRORS IN A PLANE MULTIPASS FABRY-PEROT INTERFEROMETER

A. Automatic maintenance of parallel mirrors

As we have said above, using a triple prism guarantees the parallelism of rays in working with a multipass Fabry-Perot interferometer (MFPI). Yet it is even more important in working with a MFPI to maintain the parallelism between the plane surfaces of the interferometer mirrors.

In working with the ordinary system, in which the light passes once through the interferometer, a deviation from parallelism of the mirrors leads to a strong spreading of the interference fringes and to loss of resolving power.

Whenever the light passes through the interferometer several times and in different regions of the plates, separate systems of fringes arise that more or less overlap one another, in addition to the spread of the fringes owing to non-parallelism of the plates. This greatly complicates the entire pattern, and renders the operation of the spectroscope unsuitable for research.

Hence the parallelism of the mirrors must absolutely be maintained with great accuracy over a prolonged period. This problem of maintenance is not at all easy, and in principle can be solved in two ways: 1) very refined mechanical construction and thermostating of the interferometer,[22] 2) maintenance of parallel mirrors by using automatic devices.

In practice with the MFPI, the method cited in point[1)] faces great difficulties in performance, and automatic maintenance of parallelism of the mirrors is apparently more effective. Currently two variants of automatic maintenance of parallel mirrors have been described. Ramsay[23] built an apparatus in which parallelism of the mirrors in etalons designed as light filters was maintained with high accuracy, and Sandercock[11] described another method of automatic maintenence of parallelism. In his apparatus, the interferometer was used for recording the spectral energy distribution, and we shall describe here specifically his method of automatic maintenance of parallel mirrors during the recording of the spectrum. Figure 7 shows a variant of this apparatus with a two-pass interferometer (the number of passes is of no significance here) and with an automatic system for maintaining the parallelism of the mirrors.

Laser radiation is focused with a lens onto the studied object, while the light scattered by the object is collimated into a parallel beam and directed into the Fabry-Perot interferometer. After double passage through the interferometer, as carried out with a triple prism, the studied radiation is focused onto a point dispharmg that isolates the central part of the interference pattern, and it enters a photomultiplier detector that operates in a photon-counting regime. The photopulses from the photomultiplier are applied through a preamplifier to the input of a multichannel analyzer that accumulates the results of repeated scanning of the studied region of the spectrum. To prevent the recorded spectra from being swamped by the repeated scanning owing to changed thickness of the interferometer in the intervals between successive scans, one triggers the analyzer with the most intense spectral component. In order to do this, part of the photopulses is trapped from the photomultiplier, and is applied to a pulse shaper, from which the trigger signal is applied to the trigger of the analyzer. The thickness of the interferometer is scanned by using a linear piezoelement, to which one of the mirrors of the interferometer is attached. The parallelism of the mirrors is regulated by the electric circuit shown in Fig. 7 by using X and Y piezoelectric micrometers that rotate the second mirror of the interferometer about two mutually perpendicular axes. The operation of the automatic system in adjusting the interferometer is carried out as follows. Assume that the X micrometer does not lie in the optimal position, i.e., one of the plates of the interferometer is rotated with respect to the other by some angle. Then, if sequences of square pulses of the same size, but of opposite polarity are applied to this micrometer, the plate being controlled will lie sometimes closer and sometimes farther from a parallel position. Then the electric signal, which is proportional to the intensity of the spectral component that is being recorded by the radiation detector, will differ in amplitude as the polarity of the rectangular pulse changes. When the mirrors are parallel, the amplitude of the electrical signal will not change as the polarity of the square pulse changes. In[11] this situation was used for automatic alignment of the mirrors of an interferometer parallel to one another. The logical-signal circuit shown in Fig. 7 allows automation of the process of parallel alignment of the mirrors.

The repeated scanning of the interferometer is performed by using a sawtooth pulse generator (signal *b*) by applying the pulses to the piezoelement that carries out the parallel displacement of the movable mirror. Dur-

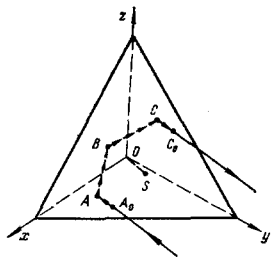

FIG. 8. Path of the rays in a triple prism. A_0 and C_0 are the entrance and exit points of the ray from the prism on the side of the xyx plane (base of the prism). A, B, and C are the points where total internal reflection of the ray occurs from the faces xOy, xOz, and zOy, respectively. O is the vertex of the triple prism, and S is the projection of the vertex on the xyz plane.

ing the forward (slow) sweep, the spectrum is recorded and information is collected on the parallelism of the mirrors, while the micrometers are corrected by means of the control signals during the reverse (fast) sweep. The square-wave generator, whose frequency is half that of the sawtooth generator, operates synchronously with the latter. During the first two scanning periods, the square-wave generator is connected to the X micrometer (signal b), while during the next two periods it is connected to the Y micrometer (signal c).

During the first and second periods of scanning the spectrum, the square-wave generator (signal b) adjusts the length of the X micrometer, and a voltage proportional to the light peak is accumulated during the first scan period in the condenser C_1, and in the condenser C_2 in the second period. The role of the switch that alternately connects the photomultiplier to the condensers is played by the pair of transistors T_1 and T_2. During the first scan period, condenser C_1 is charged through the open transistor T_1, while during the second period condenser C_2 is charged through the open transistor T_2. The alternate opening of the transistors is effected by square-wave pulses (signals g and h) whose duration is taken to be equal to that of the forward sweep of the sawtooth voltage (signal a).

Toward the end of the second scan period, when the recording of the spectrum is being completed, an opening pulse (signal d) is applied to transistor T_3 throughout the time of the reverse sweep of the sawtooth voltage. During this time, the voltage difference between the capacitors C_1 and C_2 charges the capacitor C_3 through the differential amplifier Y and the resistor R_1. The misalignment signal from the latter condenser is applied to the amplifier HV_1 having a high input impedance, and it is used for correcting the X micrometer. At the very end of the second scan period, the capacitors C_1 and C_2 are discharged through the diodes D_1 and D_2 by using a short voltage pulse (signal f), and the cycle is repeated again during the third and fourth scan periods, but now for the Y micrometer. Now the roles of the transistor T_3, resistance R_1, condenser C_3, and amplifier HV_1 are played by T_4, R_2, C_4, and HV_2, respectively.

The time constants C_3R_1 and C_4R_2 are chosen so that the final adjustment is carried out in about 10 scan periods. For a scan frequency of 1 Hz, the automatic adjustment is completed in 30 sec. As experiment has shown, a small hand correction of the X and Y micrometers is needed after several hours of operation in order to bring the operational amplifiers HV_1 and HV_2 to the middle of the working voltage range.

B. The triple prism[24]

In multipass interferometers, the mutual parallelism of the rays is ensured by using a triple prism.

A triple prism (cube corner) is a four-sided prism, three edges of which intersect at the vertex at angles of 90° with one another, while the three other edges form the base of the prism, as is shown in Fig. 8. A ray that falls on the prism on the base side passes into the prism, and after a threefold total internal reflection from its side faces, it passes back out of the prism parallel to the incident ray. The triple prism is noteworthy in that arbitrary inclinations of it with respect to the ray incident on the prism do not destroy the parallelism of the incident and reflected rays.

These properties of the triple prism are explained by the fact that the directions of the components k_z, k_y, and k_x of the wave vector are successively reversed in each of the three reflections. Thus, e.g., k_z is charged into $-k_z$ in the first reflection, k_y into $-k_y$ in the second, and k_x into $-k_x$ in the third. Thus, after the three reflections, the direction of $\mathbf{k}'$ at the point C is opposite to that of k at the point A (see Fig. 8).[3)]

The above-studied property of the triple prism fully solves the problem of establishing parallelism of the rays, and it maintains their position when mechanical influences act on the system (rocking of the prism).

The successive passes between the mirrors of the interferometer must be completely identical in optical thickness. For this reason, it is recommended that the light channels should lie symmetrically with respect to the surfaces of the interferometer mirrors.[12b] This is achieved by an appropriate adjustment of the triple prism for the two- and three-pass interferometer, while it has been proposed to use additionally a Fresnel biprism with a small deflection angle of the ray for the five-pass interferometer.[12b]

7. METHODOLOGY OF USING THE IODINE LIGHT FILTER

The vapor of molecular iodine shows in the visible a palisade of narrow and very intense absorption lines.

[3)] One can determine the geometry of the course of the rays in the studied prism by using the relationships for the coordinates of the points $A(a_x, a_y, 0)$, $B(b_x, 0, b_z)$, and $C(0, c_y, c_z)$:

$$b_x = a_x - \frac{l}{m}a_y. \quad b_z = \frac{n}{m}a_y. \quad c_y = \frac{m}{l}a_x - a_y, \quad c_z = \frac{n}{l}a_x. \tag{34}$$

Here l, m, and n are the direction cosines of the wave vector k of the incident light in the xyz coordinate system (see Fig. 8). For the most usual case of using a prism, $l \approx m$ $m \approx n \approx 1/\sqrt{3}$. Then the entrance point of the ray into the prism and the exit point of the ray from the prism lie symmetrically with respect to the projection S of the vertex O of the prism on the entrance plane.

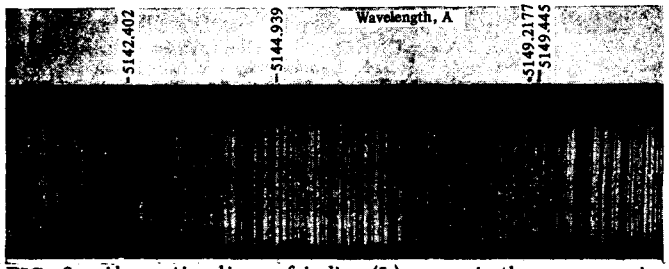

FIG. 9. Absorption lines of iodine (I_2) vapor in the green region of the spectrum.[25]

Figure 9 shows a typical absorption spectrum of iodine vapor for white light in the range 5140–5150 Å, as obtained with a diffraction spectrograph.[25] We see from Fig. 9 that the absorption spectrum of iodine vapor consists of individual narrow lines separated by rather broad intervals. The Doppler width of these lines usually amounts to several hundred megahertz, while the spacing between them is tens and hundreds of times greater than the Doppler width of the lines. The attenuation of monochromatic radiation at frequencies lying in the intervals between the absorption lines is insignificant. At the same time, the attenuation of radiation that coincides in frequency with the absorption lines of iodine can be as great as a factor of 10^8.[7] Thus a cell filled with iodine vapor can act as a high-contrast light filter that transmits radiation at frequencies that lie in the transparency region of the filter. This filter is widely applied in spectroscopy of molecular and Raman light scattering attenuate the intense radiation at the undisplaced frequency, which can distort or fully mask a spectrum being studied, owing to the nature of the instrumental profile of the spectral instrument.

Until recently, the I_2 filter had not been widely enough applied. The situation has substantially changed since the time when the authors of[7,26] used an ionized-argon laser (Ar^+ laser) for exciting light scattering, and attenuated the parasitic scattering at the undisplaced frequency with an I_2 filter by a factor of as much as 10^5 in studying Raman spectra, and as much as 10^3 in studying Mandel'shtam-Brillouin (MB) light scattering spectra. Here the useful signal was attenuated by a factor of no more than 2–4 for the MB components, and by an order of magnitude for the Raman lines.

This laser has several laser-action lines in the blue-green region of the spectrum. Henceforth we shall refer to the one having $\lambda = 5145$ Å, which overlaps a narrow absorption line of iodine vapor that corresponds to the transition $^1\Sigma_g^+ - {}^3\Pi_{0u^+}$.[7,27]

In order to make the frequency band for laser action fall within the width of the absorption line of iodine, one isolates one type of oscillation of the laser resonator, while tuning the frequency of the isolated type of oscillation to the center of the absorption line of iodine by applying passive or active stabilization.

A. Preparation of the iodine cell and the choice of its parameters

For successful application of an I_2 filter, one must pay special attention to the technique of preparing the cell and filling it with iodine. The pressure of iodine vapor in the cell is determined by the temperature of the crystalline phase, which exists in equilibrium with the iodine vapor. The cell that contains the iodine crystals is prepared of Pyrex glass, which is resistant to iodine vapor.[4)] One must thermostat the cell containing the iodine vapor for quantitative measurements of intensities of spectral components using the I_2 filter, since the intensity of the light transmitted through the filter depends exponentially on the temperature of the iodine. In order to avoid condensation of the iodine vapor on the entrance and exit windows, their surfaces are made several degrees warmer than the temperature of the walls of the cell. The parameters of the cell are its temperature, length, and diameter. The intensity of the stray and the useful radiation is attenuated by the iodine cell by the exponential law

$$I = I_0 e^{-\alpha l}, \tag{35}$$

where l is the length of the cell along the light ray, and α is the absorption coefficient. The latter has the value $\alpha_p \sim 1.25$ cm^{-1} at an iodine temperature of 80 °C for radiation at the undisplaced frequency, and $\alpha_s \sim 0.14$ cm^{-1} for the useful signal.

The contrast of the cell, as defined by the relationship

$$c = e^{(\alpha_p - \alpha_s)l}, \tag{36}$$

increases with increasing temperature, since α_p and α_s are proportional to the temperature. However, the absorption lines of iodine experience Doppler and Lorentz broadening with increasing temperature. This might lead to an undesirable loss of contrast of the filter. Therefore, the cell is generally not heated above 80 °C. In order to increase the contrast of the filter, one can expediently increase the length of the cell, if the sensitivity of the radiation detector suffices for recording the useful signal.

The contrast of the iodine filter can decline several-fold when one passes light fluxes having a high radiation density through it. Thus, at a radiation flux density of ~ 800 mW/cm^2 from a single-frequency argon laser tuned to the center of the absorption line of iodine, a cell containing iodine vapor of length 15 cm and temperature 80 °C has a contrast 10 times smaller than at a radiation density of 100 mW/cm^2. That is, absorption becomes saturated. One can avoid saturating the absorption in the iodine filter by increasing the diameter of the light flux (e.g., by using telescope systems). There-

---

4)One must not use epoxy cements to attach the windows through which the light flux passes, since the cements break down when acted on by iodine vapor. Before putting the iodine crystals in the cell, one outgasses the latter in the usual way. One fills the cell with iodine at the rate of 40 mg per cm^3 of cell volume. Before the cell is sealed, it is pumped out so as to reduce to a minimum the concentration of inert gases, which broaden the absorption lines of iodine and impair the contrast of the I_2 filter.

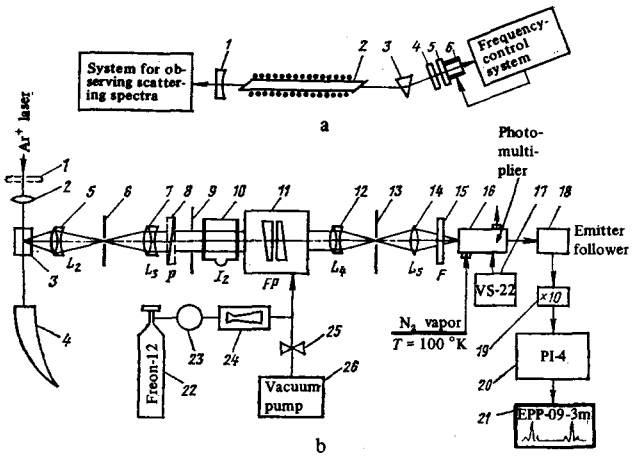

FIG. 10. Diagram of an apparatus for recording Mandel'shtam-Brillouin spectra with a single-frequency Ar^+ laser and an I_2 light filter.[31,32] a) Diagram of the single-frequency Ar^+ laser (1 and 5—resonator mirrors of the laser, 1 being curved and 5 plane); 2—gas-discharge tube with a solenoid; 3—dispersion prism; 4—quartz plate with an absorbing film; 6—piezoceramic element); b) elements of the interference apparatus and spectral recording by the photon-counting method (1—plate to rotate the polarization of the laser radiation, 2—focusing lens (f = 200 mm), 3—crystal under study, 4—Wood's horn, 5—intermediate objective (f = 59 mm), 6—entrance aperture, 7—collimator (f = 160 mm), 8—polarizer, 9—aperture diaphragm, 10—cuvette containing I_2 vapor, 11—hermetically sealed chamber containing the Fabry-Perot interferometer, 12—objective (f = 270 mm), 13—exit aperture, 14—lens (f = 50 mm), 15—green light filter, 16—radiation detector (photomultiplier) cooled with vapor of liquid nitrogen and having magnetic defocusing, 17—power supply, 18—emitter follower, 19—preamplifier, 20—PI-4 linear intensimeter; 21—recorder, 22—gas cylinder, 23—reducing valve, 24—supersonic nozzle, 25—valve, 26—pump).

fore one should choose the diameter of the iodine cell so that the light does not cause the absorption to saturate.

B. Stabilization of the frequency of an Ar^+ laser at the iodine absorption line. Description of the working apparatus

The laser frequency must be stabilized in order to maintain it at the center of the absorption line of iodine during recording of the scattered-light spectra.

We shall treat only the most usual methods of active stabilization of the frequency of an Ar^+ laser, which are based on using feedback circuits. The fast action of the stabilizing device and its operational quality are determined in many ways by the design and type of dispersion element that selects the single mode of oscillations, as well as by the shape of the discrimination profile over which the frequency stabilization is performed. In[7], a single mode of oscillation of the resonator of an Ar^+ laser was selected by using a quartz plate made in the form of a Fabry-Perot etalon, and placed inside the laser resonator at a small angle to its axis. The iodine filter itself served as the discrimination profile in this study. The laser frequency was tuned to the transmission minimum of the iodine filter, which had a temperature of ~ 80 °C. The laser frequency was stabilized at the center of the iodine absorption line by varying the temperature of the quartz plate. This method of frequency stabilization shows inertia, and this is its defect.

Fast-acting methods of stabilizing the frequency of an Ar^+ laser by using iodine vapor as the frequency discriminator have been developed in[28,29]. A single mode of oscillation of the Ar^+ laser was selected in[28,29] by using a Smith resonator whose frequency was tunable by a piezoelectric method. In[28], the frequency of the selected mode of oscillation was stabilized at the absorption line of the iodine vapor in the cell, and in[29], at the resonance fluorescence line of a beam of I_2 molecules.

A method based on using a thin, light-absorbing film shows a number of advantages over the other methods for selecting the modes of oscillation of an Ar^+ laser. This method has been proposed and carried out by Troitskiĭ.[30] One mode of oscillation of an Ar^+ laser was selected by using a film in[31], and its frequency was stabilized at the center of an absorption line or resonance flourescence line of iodine vapor in a cell placed outside the laser resonator.

The selecting action of a thin absorbing film is based on the idea that it selects from among all the modes of oscillations of the laser resonator the one that has a standing-wave node at the surface of the film. The free spectral range of the equivalent interferometer that the film forms with its nearest blind mirror of the laser resonator can be made one or two orders of magnitude larger than in the three-mirror Smith resonator, while the construction and tuning of this interferometer are incomparably simpler. It was shown in[31] that one can get the greatest effect in reliable stabilization of the frequency of an Ar^+ laser by tuning the laser frequency to the maximum of the resonance fluorescence line of I_2 vapor. In order to decrease the width of the fluorescence line, one can expediently use a cold (room-temperature) iodine cell. Thus one needs two iodine cells: one (cold) one is used to stabilize the frequency at the resonance fluorescence line, and the other (hot) one is used as a high-contrast filter.

Figure 10 shows a diagram of the instrument used in[31]. Its fundamental parts are the Ar^+ laser, the frequency-control system, and the system for observing the scattering spectra. The Ar^+ laser (Fig. 10a) included a gas-discharge tube of the type DARK-12000. The design of the gas-discharge tube of this Ar^+ laser has been described in detail in[33]. A single-frequency laser-action regime with this tube was first achieved in[34].

Laser action with a single mode of oscillation of the resonator was achieved by using a thin absorbing film made of nichrome (the transmission of the film at λ = 5145 Å was 73%). The latter was deposited onto a plane quartz plate having an antireflection coating. The plate was placed inside the laser resonator at a distance of 15 mm from the plane mirror. This mirror was attached to a piezoceramic element, which tuned the laser frequency by changing the distance between the film and the mirror. The power of the laser in a single-frequen-

cy mode near the center of the amplification line amounted to ~ 400 mW.

One can use either photographic or photoelectric recording to observe molecular light-scattering spectra using the I_2 filter. Figure 10c shows the system of photoelectric recording of MB spectra that was described in detail in[32].

We should list among the faults of the I_2 filter the existence of additional narrow absorption lines (see Fig. 9), which can overlap the spectral components of the fine structure of the Rayleigh line.

We note that the I_2 filter can distort only the intensity distribution of the components in the MB spectra of crystals, without substantially affecting the positions of their maxima, since the MB components that are excited in a crystal by a single-frequency laser are considerably narrower than the absorption lines of I_2.

In order to elucidate the true nature of an MB scattering spectrum, one should record the spectrum either while changing the direction of recording of the scattered light, or while rotating the studied crystal through a small angle about the direction of the light incident on the crystal. In both cases, the frequencies of the MB components are altered because of the change in the frequency of the phonon that participates in the light scattering: in the former case, owing to the change in the scattering angle, and in the latter, owing to the anisoropy of the velocity of sound in the crystal.

The examples of application of multipass and tandem interferometers and of the iodine cell to the physical studies cited below primarily are aimed to illustrate the experimental potentialities of these applications, while we have discussed the physical results often to a far smaller degree than they deserve.

8. SOME RESULTS OF STUDYING MOLECULAR LIGHT-SCATTERING SPECTRA USING THE MULTIPASS OR TANDEM FABRY-PEROT INTERFEROMETER

A. Studies of light-scattering spectra in phase transitions in imperfect crystals

Sandercock[11] first applied a double-pass Fabry-Perot interferometer for studying the molecular light-scattering spectrum in an antimony sulfoiodide crystal (SbSI). At $\lambda = 6328$ Å, the SbSI crystal has an absorption coefficient for light of 10^2–10^3 cm^{-1}, depending on the direction of polarization of the exciting and the scattered light with respect to the crystallographic directions. He studied light that was scattered from the natural faces of the crystal at an angle of 180°.

Figure 11 shows a recording of the spectrum of the fine structure of the Rayleigh light-scattering line in an SbSI crystal in two adjacent interference orders. The upper curve was obtained by recording the spectrum of the scattered light with a single-pass (ordinary) interferometer. One can see on the curve the Mandel'shtam-Brillouin (MB) components due to a longitudinal elastic thermal wave on a huge background arising from the "tail" of the undisplaced line. The undisplaced line is

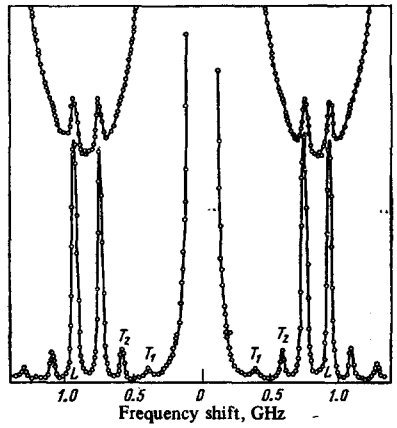

FIG. 11. Mandel'shtam-Brillouin spectra of an SbSI crystal.[11] Spectrum obtained with a single-pass FPI (upper curve) and that obtained with a double-pass FPI (lower curve) (T_1 and T_2 are the transverse and L the longitudinal components; the unmarked components belong to the next order of the spectrum).

very intense, owing to the large amount of stray light. The lower curve is the recording of the spectrum of the same scattered light using a two-pass Fabry-Perot interferometer. The intensity of the stray light has remained the same, yet the contrast has risen so strongly that one can distinctly see the MB components due to the longitudinal waves L and the fast and slow transverse waves T_1 and T_2. These latter components were not at all visible in analyzing the spectrum of the scattered light with a single-pass interferometer. The nine elastic constants of the SbSI crystal were determined from the positions of the MB components and from measurements of the refractive index in different crystallographic directions.

The elastic constants differed only slightly at temperatures above the ferroelectric transition of SbSI (t_c = 19 °C) and below it (at 22° and 12 °C, respectively). However, careful study of the vicinity of the phase-transition point with light scattering excited with a He–Ne laser of 80 μW power revealed an abrupt change in the elastic constants in a temperature range of 0.25 °C.

Fine-structure spectra in a crystal of gadolinium molybdate ($Gd_2(MoO_4)_3$) have been determined in[35,36] with the purpose of studying the behavior of the elastic constants in the ferroelectric phase transition. They used a tandem combination of interferometers having identical thickness (to an accuracy of $\lambda/4$) and differing finesse factors. Figure 12 shows a diagram of the tandem arrangement of the interferometers. The spectrum was recorded by varying the air pressure in the interferometer chambers. The finesse in one interferometer was 35, but only 12 in the other. The overall finesse amounted to about 35. The contrasts of the interferometers also differed, being 2500 and 100, respectively. According to Eq. (32), the resultant contrast should amount to 25×10^4, though it amounted to only 7×10^4, for reasons not clear to the authors.[35,36] Yet even this contrast sufficed to solve the problem formulated above.

Figure 13 shows recordings that permit us to compare

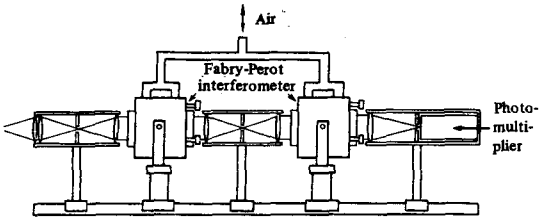

FIG. 12. Diagram of a tandem combination of two interferometers. The spectrum is scanned by varying the pressure.[36]

how the spectra look from the single interferometer and from the tandem combination.

The studied crystal of gadolinium molybdate is a ferroelectric having a phase-transition temperature t_c = 159 °C. Above t_c (paraelectric phase), the crystal is tetragonal with the space group D_{2d}^3. Below t_c (ferroelectric phase), the crystal is orthorhombic with the space group C_{2v}^8.

They found the elastic constants C_{11} and C_{22} from the size of the displacement of the MB components arising from longitudinal ultrasonic waves propagating along the orthorhombic x and y axes. The longitudinal ultrasonic waves that propagate at a 45° angle to the x and y axes are responsible for the longitudinal MB components from whose positions the constant C'_{11} was determined.

We see from the relationships shown in Fig. 14a that the modes[5] that correspond to C_{11} and C_{12} "soften" as we approach the phase-transition point. The same is also true of the mode C'_{11} (which is not shown in the diagram). The mode C_{11} varies especially strongly with the temperature. The damping of the modes C_{11} and C_{22} was also determined in[35,36] from the width of the MB components. Figure 14b shows the results of these measurements. We see from the diagram that the damping of the modes increases greatly as we approach the phase-transition point, and the effect of increased damping is especially strongly marked for the mode C_{11}. For this mode, the damping at 159 °C exceeds by a factor of eight its value at 140 °C. This study contained no physical discussion of the obtained results. The authors intend to do this later. They only remark that an interaction of optical and acoustic phonons is responsible for the observed anomalies in the elastic constants. Several careful experimental studies have been made of phase transitions in crystals of rare earth vanadates, which are especially suitable objects for studying Jahn-Teller phase transitions (see[37] and the literature cited there).

Sandercock *et al.*[38] have carried out a difficult experimental study of Mandel'shtam-Brillouin spectra in dysprosium vanadate ($DyVO_4$) and terbium vanadate ($TbVO_4$). The dimensions of the studied crystals were 1×1×4 mm, while the faces and volumes of the crystals contained defects that gave rise to a large amount of

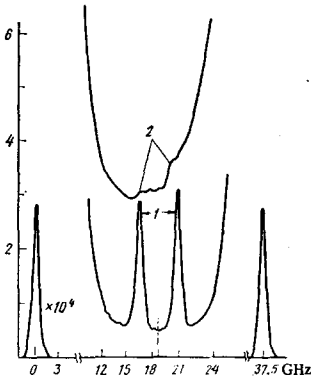

FIG. 13. Recording of a spectrum of a $Cd_2(MoO_4)_3$ crystal.[35,36] 1—With one interferometer, 2—with a tandem combination of two interferometers.

stray light. The studies were even further complicated by the need to work at low temperatures, including liquid-helium temperatures, at which the intensity of molecular light scattering is infinitesimally small. On the other hand, the intensity of the light that excites scattering must not be large, so as not to overheat in an uncontrollable way the volume in which the phase transition is being studied.

The study owed the successful overcoming of all these vast experimental difficulties to the application of a multipass Fabry-Perot interferometer.

The $DyVO_4$ and $TbVO_4$ crystals were put into a cryostat where their temperatures could be varied from 4.2 to 300 °K.

The phase-transition temperature of $DyVO_4$ is 14 °K, while that of $TbVO_4$ is 34 °K. Above the phase-transition temperatures, the crystals are tetragonal in structure (D_{4h}). Below the phase-transition temperatures, the crystals have orthorhombic structures (D_{2h}).

The light scattered at an 180° angle from the incident light was directed into a multipass Fabry-Perot interferometer. They chose to observe the scattered light at a 180° angle because the broadening of the MB components owing to the finite angle of observation is insig-

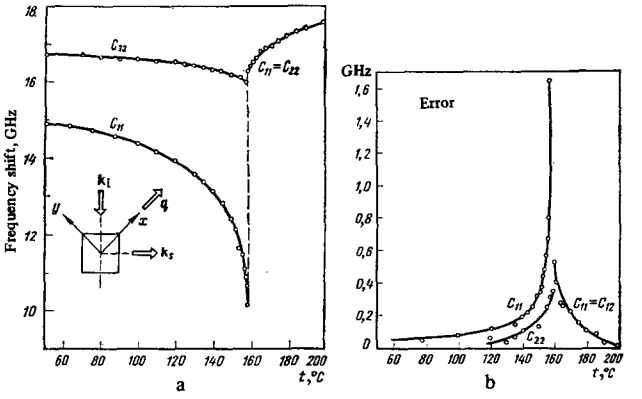

FIG. 14. Positions of the components and the damping of ultrasound in a $Cd_2(MoO_4)_3$ crystal.[35,36] a) Temperature-dependence of the positions of the MB components; b) Temperature-dependence of the widths of the MB components.

[5]Hereinafter, the modes C_{11}, C_{22}, and C'_{11} (or henceforth $c_{11}-c_{12}$) are taken to mean the polarized acoustic vibrations of the crystal produced by a sound wave whose phase velocity is governed by the given elastic constant (or given combination of elastic constants).

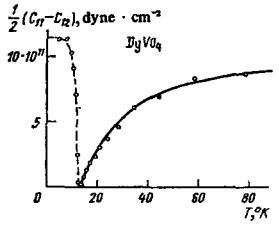

FIG. 15. The nature of the "softening" of the elastic constant $(C_{11}-C_{12})/2$ in the vicinity of the phase transition in a $DyVO_4$ crystal.[38]

nificant at this scattering angle. Thus one can increase considerably the aperture of the detecting system as compared with the aperture of a system used for 90° scattering.

In[38], the speed of sound was determined from the displacement of the MB components by the formulas of[1], and the softening of particular modes during the phase transition was traced from the variation in the speed of sound.

They could observe in the $DyVO_4$ crystal the softening with varying temperature of the mode $(C_{11}-C_{12})=2\rho v_T^2$ (v_T is the velocity of transverse waves) near the phase-transition point, while the direction of propagation was 25° from the [110] direction (Fig. 15).

In studying the spectrum of $TbVO_4$ in the region of the phase transition, they observed softening in the mode governed by the elastic constant $C_{66}=\rho v_T^2$, in which the direction of propagation of the sound wave was 12° from the [100] direction. Here C_{66} declined strongly at the phase-transition point. It also turned out that this constant depends on the frequency of the sound.

One can find a theoretical description and further experimental details in the original papers[37,38] and the literature cited there.

It is essential to stress here that the "soft" mode is softened so much in both crystals that the corresponding elastic constants can vanish. This essential result for ultrasonic frequencies was obtained from the Mandel'shtam-Brillouin spectra, owing to the new high-resolution spectroscopic methods.

This technique has also proved to be very effective in studying such phenomena as a phase transition from isotropic liquid to liquid crystal and phase transitions between liquid-crystalline structures. As an example of effective use of a two-pass Fabry-Perot interferometer to study scattered-light spectra in a liquid crystal, we point out the study by Pershan and his associates.[39]

In this study, they studied molecular light-scattering spectra in a single-domain specimen of β-methyl butyl *p*[(*p*-methoxy benzylidine)-amino]cinnamate. The liquid crystal was placed between glass plates that had been treated with lecithin. The distance between the plates was 250 μm. The specimen was heated to 99.6 °C (isotropic phase). Upon slow cooling, they successively got specimens of the nematic phase (99.6–81.0 °C), the single-domain smectic *A* phase (81.0–59.8 °C), and the single-domain uniaxial *B* phase ($T<59.8$ °C). Below 47.0 °C, the smectic *B*-phase was rapidly quenched so as to avoid formation of polycrystallinity.

The scattered light was excited by light of $\lambda=5145$ Å from an argon laser of power not exceeding 200 mW, in order to prevent heating and photochemical damage to the specimen. The value of the wave vector $\mathbf{q}=\mathbf{k}_s-\mathbf{k}_i$ (where $\mathbf{k}_i$ and $\mathbf{k}_s$ are the wave vectors of the exciting and scattered light, respectively) was varied in this experiment by a factor somewhat less than two.

Figure 16 shows recordings of the spectrum in different polarizations at different temperatures. They determined from the spectra the velocities and polarizations of the ultrasonic waves, and they measured the thermodynamic quantities that describe the relationship between the density and arrangement of layers in smectic crystals having $C_{11}-C_{13}\neq 0$. It was clearly established that $C_{44}\neq 0$ in the smectic *B* phase.

B. Studies of light-scattering spectra in opaque crystals and metals. Scattering of light by acoustic magnons

Whereas Raman spectra in opaque media and powders have been studied also recently by using high-contrast double and triple spectrometers, the MB spectrum could not be studied under the same conditions.

Now with the appearance of multipass Fabry-Perot interferometers, such studies have proved to be possible, as has been pointed out above, and were first carried out in[11]. Sandercock[19] has likewise been responsible for the development of these studies, having studied the MB spectrum in the opaque crystals of silicon (Si) and germanium (Ge). In these substances, the absorption coefficient lies in the range between 10^4 and 6×10^5 cm^{-1} for wavelengths of light of 6328 and 4880 Å, respectively. The problem of how the absorption of the exciting and the scattered light affects the widths of the MB components was treated in[19]. Wehner[40] has treated this problem in general form, and it turned out that the width of the Mandel'shtam-Brillouin components

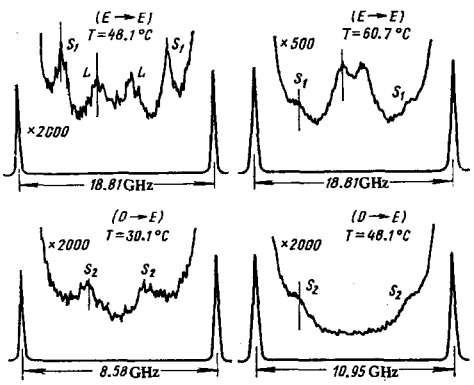

FIG. 16. Mandel'shtam-Brillouin spectra in a smectic liquid crystal (β-methyl butyl *p*-anniocinnamate).[39] Designations of the spectra: $E\rightarrow E$—the incident and scattered light are polarized as the extraordinary wave, $O\rightarrow E$—the incident light is polarized as the ordinary wave, and the scattered light as the extraordinary wave. S_1 and S_2—shear (transverse) components, *L*—longitudinal components.

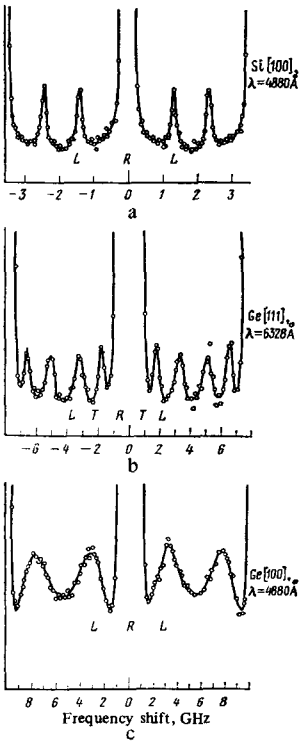

FIG. 17. Mandel'shtam-Brillouin spectra of opaque crystals obtained at a scattering angle $\theta = 180°$.[19] a) Silicon crystal, direction of ultrasound along [100], $\lambda = 4880$ Å; b) germanium crystal, direction of ultrasound along [111], $\lambda = 6328$ Å; c) germanium crystal, direction of ultrasound along [100], $\lambda = 4880$ Å. L—longitudinal, and T—transvers components. The unmarked components belong to adjacent orders of the spectrum.

will practically completely depend on the absorption of light, rather than on the absorption of sound, as in the case of light scattering in transparent dielectrics.

The conclusions of[40] imply that the half-width of the MB components will be

$$\bar{\Gamma}_g = \Gamma_g + vq\frac{n_2}{n_1}, \quad n = n_1 + in_2, \tag{37}$$

where Γ_g is the half-width of the MB components in the absence of light absorption, $q = 2n_1k_0\sin(\theta/2)$, and n_2 and n_1 are the imaginary and real parts of the refractive index, respectively.

Equation (37) implies that the width of the MB components is practically completely determined by the second term, and hence, by light absorption. Actually, the second term in (37) exceeds the first at room temperature by almost three orders of magnitude, while the role of the second term increases even more at lower temperatures. Thus, one can determine from the scattering spectrum in an opaque crystal such an important constant as n_2, or in other words, the absorption coefficient for light.

The experiment of[19] used the light of the line $\lambda = 6328$ Å at power 20 mW and of $\lambda = 4880$ Å at power 200 mW. The scattered light passed through a Fabry-Perot interferometer of contrast about 10^9, and was received by a photomultiplier whose dark current amounted to only 1/2 pulse per second. Measurements were performed on surfaces of silicon and germanium crystals oriented in the crystallographic directions [100] and [111]. The surfaces were required to be of very high optical quality. Whereas commercial specimens of silicon had surfaces of excellent quality, the surfaces for germanium were unsatisfactory. The author was able to get better results by etching the surfaces. Yet even in this case, the stray light was so strong that it overheated the photocathode of the photomultiplier. Therefore the frequency of scanning was reduced to 10 per minute.

The light that excited the scattering somewhat overheated the studied specimen. However, this heating did not exceed 30° as estimated by the author of[19].

Figure 17 shows typical recordings of spectra. We can distinctly see on the spectra the effect of light absorption. Thus, in Fig. 17a for a case in which the absorption coefficient for light is 10^4 cm^{-1}, the ratio of the width of an MB component to its displacement is only about 3%. In Fig. 17b, where we simultaneously observe longitudinal and transverse components, we see that the longitudinal components are broader than the transverse ones, as we should expect from (37) for $v_L > v_T$.

Figure 17c shows a recording of a spectrum in which the absorption coefficient for light is 6×10^5 cm^{-1}, and the ratio of the width of the MB component to its displacement is approximately 100%. Processing of the spectra (Fig. 17) with account taken of the instrumental profile permitted finding the quantities n_1 and n_2. In calculating n_1, the speed of sound was assumed to have the known ultrasonic value. Table I gives the results of measuring the quantities n_1 and n_2.

Dil and Brody[45b] have recently obtained Mandel'shtam-Brillouin spectra in the liquid metals mercury and gallium.

In contrast to dielectrics and semiconductors, which were discussed above, the thermodynamic density fluctuations in metals modulate not only the dielectric constant, but also the electric conductivity. This is because the longitudinal displacements of the ions perturb the states of both the bound and the free electrons. Here the charge neutrality in liquid metals under longitudinal vibrations of the ions is maintained by electromagnetic coupling between the ions and the free electrons, up to the plasma-oscillation frequencies. Since the optical constants in metals are mainly determined by the elec-

TABLE I.

λ,Å	Direction and mode	n_1		n_2	
		Ref. 19	Other studies	Ref. 19	Other studies
			Silicon		
6328	[100] L	3.89	3.92[a]		
	[100] T	3.92			
4830	[100] L	4.38		0.06	0.051[b]
	[111] L	4.35	4.36[b]	0.07	
			Germanium		
6328	[100] L	5.56		0.67	
	[111] L	5.61	5.53[c], 5.43[d]	0.70	0.69[c], 0.82[d], 0.85[e]
	[111] T	5.55		0.65	
4880	[100] L	5.76	4.55[c], 4.31[d]	2.38	2.56[c], 2.30[d], 1.55[c]

Refs. a, b, c, d, and e denote Refs. 41, 42, 43, 44, and 45a, respectively

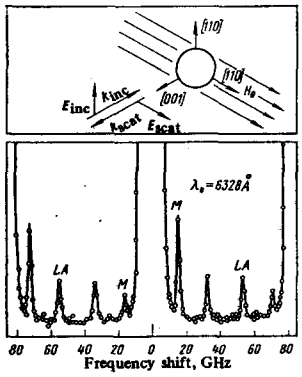

FIG. 18. Mandel'shtam-Brillouin and magnon light-scattering spectra in yttrium iron garnet ($Y_3Fe_5O_{12}$).[46] L—longitudinal MB components, M—magnon componnnts. The unmarked components belong to adjacent orders of the spectrum. The geometry of experiment in which the given spectrum was obtained is shown at the top.

tric conductivity, the ion-density fluctuations are manifested in such a way that the MB scattering in a metal is mainly determined by the free electrons.

In order to get the MB spectra, Dil and Brody used a five-pass plane FPI having a contrast greater than 10^{12}, a finesse of 80, and 20% transmission at a wavelength of 5145 Å.

They determined from the position of the MB components the velocity of ultrasound (at frequency 3×10^9 Hz), which proved to be $v_{Hg}=(1.75\pm0.15)\times10^5$ cm/sec and $v_{Ga}=(1.90\pm0.30)\times10^5$ cm/sec.

A good example of applying the technique of the multipass Fabry-Perot interferometer for studying thermal magnetoelastic waves from the Mandel'shtam-Brillouin spectrum has been given by studies of Sandercock and Wettling[46] and Sandercock.[47]

In ferromagnetic and antiferromagnetic crystals, which show magnetic order, strong coupling exists between the spin orientations of the individual atoms.

This orienting interaction gives rise in these substances to spin waves or magnons.[48]

The frequency of the spin waves is expressed by the relationship

$$\omega_{sp} = Dq + \gamma H. \tag{38}$$

Here D, q, γ, and H are the exchange parameter, the wave vector of the magnon, the gyromagnetic ratio, and the magnetic field in the specimen.

The frequency of the acoustic thermal waves is expressed by the well-known simple relationship

$$\Omega = vq, \tag{39}$$

where v is the speed of sound.

The spin waves and the acoustic (elastic thermal) waves are mutually coupled by the phenomenon of magnetostriction. This coupling gives rise to a magnetoelastic wave that modulates the scattered light. Hence, besides the components due to the purely elastic longitudinal and transverse waves, the scattered-light spectrum should also contain components due to the magnetoelastic waves, or as they are also called, acoustic magnons. Until recently, such components had not been observed in the thermal Mandel'shtam-Brillouin scattering spectrum of antiferromagnetics. Only diffraction of light by an artificially created magnetoelastic wave had been observed.[49,50]

A line in the thermal Mandel'shtam-Brillouin scattering spectrum arising from a thermal magnetoelastic wave in yttrium iron garnet ($Y_3Fe_5O_{12}$) could be observed for the first time in the above-cited study by Sandercock and Wettling.[46] They used a five-pass Fabry-Perot interferometer in the study. The scattered light was excited with the radiation of He–Ne and Ar^+ lasers with the wavelengths $\lambda=6328$, 5145, and 4880 Å. Since the crystal was opaque at these wavelengths, they had to restrict the emission powers of the lasers to 10–20 mW, and the scattered light was observed in the backward direction (scattering angle $\theta=180°$) with the specimen at room temperature. The specimen crystal of $Y_3Fe_5O_{12}$ was prepared in the form of a sphere.

Figure 18 shows the scattered-light spectrum. The directions of the wave vectors of propagation, the polarizations of the incident and scattered light, and the direction of the external magnetic field are indicated here. Calculation shows that the position of the peak of the magnon component in the scattered-light spectrum for the case in which the wave vector q is perpendicular to the direction of the external magnetic field is determined by the expression[46,47,51]

$$\omega_{sp}^2=\gamma^2\left(H_0+H_{an}-\tfrac{4}{3}\pi M_0+Dq\right)\left(H_0+H_{an}-\tfrac{4}{3}\pi M_0+Dq^2+4\pi M_0\right). \tag{40}$$

Here H_{an} is the anisotropy field, $(4/3)\pi M_0$ is the demagnetization field, and M_0 is the magnetization at saturation. In calculating ω_{sp} from the concrete values used in[46], the position of the magnon component agreed well with the experimental data.

The other study[47] treated a $CrBr_3$ crystal over a broad range of temperatures including the lower Curie point $T_c=32.5$ °K. The crystal was cut in the form of a plate, and light of the wavelength $\lambda=4880$ Å, for which the crystal was practically transparent, was used to excite the scattered light. The scattering angle θ amounted to 180° or 20°. A five-pass Fabry-Perot interferometer was used as the spectral apparatus. The spectrum of Fig. 19 shows the Stokes and anti-Stokes magnon components as well as the longitudinal acoustic Mandel'shtam-Brillouin components.

This study treated not only the position of the magnon components, their intensities, and their temperature kinetics, but also the lifetime of the magnons. For this latter problem, a spherical interferometer having a dispersion region of 325 MHz was set up following the five-pass interferometer having the free spectral range of 76 GHz. The width of the instrumental profile of the

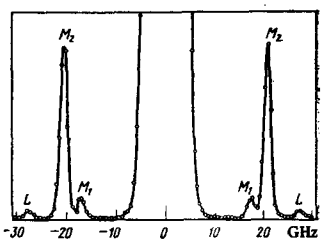

FIG. 19. Mandel'shtam-Brillouin and magnon light-scattering spectra in a $CrBr_3$ crystal.[47] L—longitudinal MB components, M_1 and M_2—magnon components.

apparatus was ~ 10 MHz, while its contrast was as high as $\sim 10^{12}$.

With a spectral apparatus having these record-breaking characteristics, the width of the magnon line was measured in the temperature range from liquid helium to ~ 30 °K, and it proved to lie in the range from ~ 40 to 150 MHz.

Wettling *et al.*[51] have developed a detailed theory of the phenomenon, including intensity problems.

C. Some special cases

The high contrast of the five-pass interferometer permitted Sandercock[52] to study the Mandel'shtam-Brillouin spectrum in thin films of collodion and Mn_2PS_4 with backward light scattering.

For thin films, the molecular light-scattering spectrum acquires interesting features. At a film thickness d of the order of the wavelength of the light wave, the MB components of the light scattered at an angle of 180° are broadened, and they acquire a shape of the type $(\sin^2 x)/x^2$, with a half-width $\delta\Omega = \Omega_0\lambda/2nd$, where $x = (\Omega_0 - \Omega)d/2v$, Ω_0 is the frequency at the peak of the MB component for the massive material, and λ is the wavelength of the exciting light.[52] The intensity of the scattered light will be modulated by the frequencies of the phonons $\Omega_s = p\pi v/d$, where p is an integer, and v is the speed of sound in the material of the film. This modulation will vary in depth, depending on the absorption coefficient of ultrasound and the thickness of the film. Figure 20 shows the results of experimental observation. If we consider that the film can be extremely thin ($d < 10^{-5}$ cm), the half-width $\delta\Omega$ can become greater than Ω_0, and thus the spectrum of the studied phonons can be extended to frequencies greater than 100 GHz. The possibilities of using thin films for creating a phonon spectrometer are also discussed in[52].

By using a three-pass Fabry-Perot interferometer having a contrast ~ 10^6, they have studied in[53] the Mandel'shtam-Brillouin spectrum in polycrystalline specimens of Irtran-3 formed from monocrystals of CaF_2 of dimensions ~ 150 μm, and pressed at high temperature *in vacuo*.

They used an Ar^+ laser of wavelength $\lambda = 4880$ Å and emission power from 0.5 to 1.5 W to excite scattered light in Irtran-3. Even when the scattered light was observed at an angle of 90°, the stray light arising from inclusions and pores in the specimen was so strong that it ruled out the possibility of recording Mandel'shtam-Brillouin spectra with a single-pass Fabry-Perot interferometer. The studied scattering volume amounted to 50 μm in length and 20–28 μm in diameter. This permitted them to observe scattering from individual monocrystals in the specimen, and to determine from the form of the MB spectrum the mutual orientation of the individual monocrystals. It turned out that the intensity of the stray light does not grow catastrophically when boundaries of the monocrystals fall within the scattering volume. This means that the inclusions and pores in the studied polycrystalline specimen are not concentrated at the boundaries of the monocrystals.

As the presented examples make clear, multipass Fabry-Perot interferometers permit one to study objects under conditions such as are not attainable to study by single-pass interferometers.

Multipass interferometers are also applied with great success for refining substantially the elastic- and elasto-optic constants and damping coefficients for ultrasound.

Examples of such successful studies are those of Grimsditch and Ramdas[54] and of Pelous and Vacher.[55] The first of these studies applied a three-pass interferometer to get the Mandel'shtam-Brillouin spectrum in natural diamond crystals. From these spectra, they obtained the elastic and elasto-optic constants in Table II, and the values of these constants that had been obtained in earlier studies[56,57] were refined.

Pelous and Vacher[55] used a tandem combination of a two-pass plane Fabry-Perot interferometer and a one-pass spherical one. Figure 21 shows a diagram of their apparatus. They studied with this apparatus the speed and absorption of ultrasound in fused quartz over the temperature range from liquid helium to room tempera-

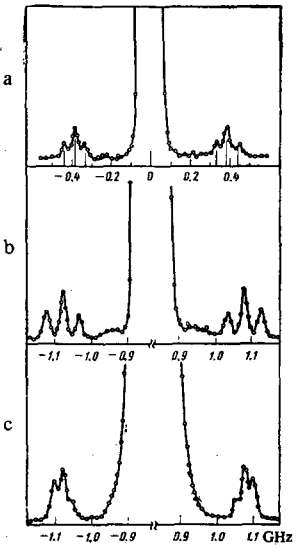

FIG. 20. Spectra of light scattering at 180° in thin films.[52] a) Sextet of longitudinal MB components in collodion; b) sextet of longitudinal MB components in Mn_2PS_4 (film thickness 1.1 μm); c) sextet of longitudinal MB components in Mn_2PS_4 (film thickness 2.0 μm).

TABLE II. Elastic and photoelastic constants of diamond.

Elastic constants × 10^{-12}, dyne/cm²:*			Photoelastic constants		
C_{11}	C_{12}	C_{44}	P_{11}	P_{12}	P_{44}
10.76±0.002	1.25±0.02	5.77±0.01	−0.249	0.043	−0.172

*A density $\rho = 3.512$ g/cm³ was assumed in calculating the elastic constants, while the refractive index for the wavelength λ was determined from the relationship

$$n^2-1=\frac{\varepsilon_1\lambda^2}{\lambda^2-\lambda_1^2}+\frac{\varepsilon_2\lambda^2}{\lambda^2-\lambda_2^2},$$

where $\varepsilon = 0.3306$, $\varepsilon_2 = 4.3356$, $\lambda_1 = 0.175$ μm, and $\lambda_2 = 0.106$ μm.

ture. They established an absorption maximum in the vicinity of 80 °K and the frequency-dependence of the absorption coefficient on both sides of the maximum.

9. SOME RESULTS OF STUDYING LIGHT-SCATTERING SPECTRA USING THE IODINE LIGHT FILTER

The first practical application of the iodine light filter was that of Peticolas, Hibler, *et al.* [59] to study Raman spectra in a single crystal of polyethylene, and of Devlin, Davis, *et al.* [7] to study Raman spectra in a crystal of gadolinium molybdate $Gd_2(MoO_4)_3$ and the Mandel'shtam-Brillouin scattering spectrum in a monocrystal of magnesium oxide MgO.

Figure 22 shows the MB spectra in the MgO crystal. The upper diagram pertains to the spectrum recorded without an I_2 filter, and the lower one with the I_2 filter. Without the I_2 filter, the stray light at the undisplaced frequency completely masked the MB components.

The I_2 filter attenuated the stray light by a factor of 500, and made it possible to observe distinct MB components.

In[60], they obtained with an I_2 filter MB spectra in a cholesteric liquid crystal that amounted to a mixture of three cholesteric crystals, and they studied the variation in the acoustic properties of this crystal during the phase transition from the liquid to the liquid-crystalline state.

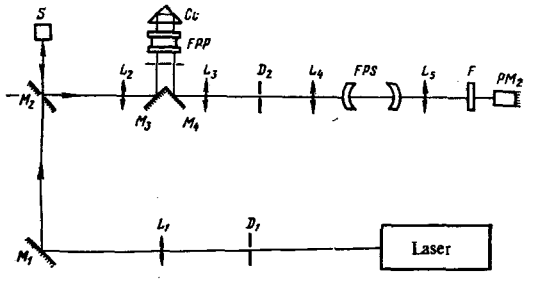

FIG. 21. Diagram of an experimental apparatus for studying the positions and widths of MB components in fused quartz.[55] L_1—focusing lens, M_1—rotatable mirror, M_2—rotatable mirror with a hole, S—specimen under study, L_2—collimating lens, M_3 and M_4—rotatable mirrors, FPP and Co—double-pass Fabry Perot interferometer with a triple prism, L_3—focusing (camera) lens, D_2—intermediate diaphragm, L_4—collimator, FPS—spherical Fabry-Perot interferometer, L_5—focusing (camera) lens, F—filter, PM_2—radiation detector (photomultiplier).

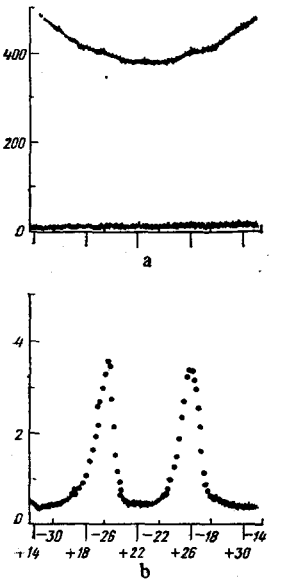

FIG. 22. Mandel'shtam-Brillouin spectra in an MgO crystal.[7] a) Without using an iodine light filter; b) using an iodine light filter. The spectrum of Fig. b shown longitudinal MB components, with the Stokes component at the left and the anti-Stokes at the right.

They prepared a specimen having rather large domains for the studies: the dimensions of the domains exceeded the wavelength of the ultrasound by a factor of about 1000. The specimen was prepared in the form of a thin layer lying between two glass plates that had been smeared with lecithin in order to put the specimen into the monodomain state. The thickness of the layer was 250 μm.

The intensity of the stray light exceeded that of the MB components by seven orders of magnitude. They were able to record in this study the MB spectra with a Fabry-Perot interferometer that had an intrinsic contrast of ~ 10^3 only by using an I_2 filter. Figure 23 shows a diagram of the experimental apparatus, and Fig. 24 shows a spectrum obtained with it. We see from the spectrum that the intensity of the Stokes MB component is distorted by one of the absorption lines of iodine, while the anti-Stokes component is practically undistorted, and the authors[60] used it to measure the acous-

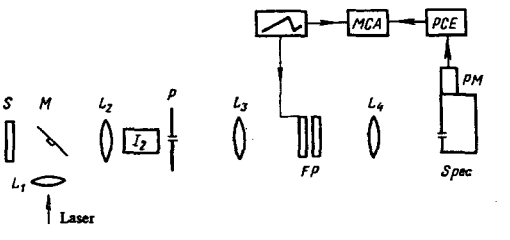

FIG. 23. Diagram of an apparatus for observing MB spectra in liquid crystals.[60] L_1—focusing lens, M—micromirror, S—object under study, L_2—intermediate lens followed by the cell containing iodine vapor, P—diaphragm, L_3—collimator, FP—piezoelectrically-scanned Fabry-Perot interferometer, L_4—camera lens, Spec—monochromator, with the radiation detector (PM) placed at its output, and the signal from the latter applied to a multichannel analyzer. The analyzer is triggered by an external generator, just as the interferometer is.

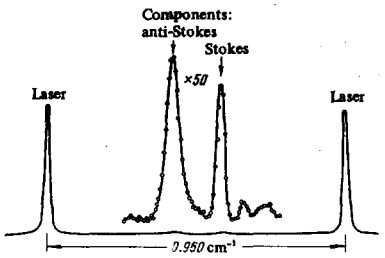

FIG. 24. Mandel'shtam-Brillouin spectrum of a cholesteric liquid crystal (34% cholesteryl oleyl carbonate, and 32% cholesteryl cholride) at 20 °C.[60] The Stokes component and the background are distorted by extra absorption lines of iodine.

tic parameters of the liquid crystal.

The iodine light filter has been successfully applied to study MB light-scattering spectra in optically imperfect crystals of solid solutions of ZrO_2–Y_2O_3.[61] The studies were performed on crystals containing from 10 to 20 mole percent Y_2O_3 in the apparatus discussed in Sec. 7 of this article. The studied specimens of the single crystals were cut in the shape of parallelepipeds whose three mutually perpendicular edges were oriented along the twofold and fourfold axes. The length of the edges was 3–8 mm. Figure 25 shows typical light-scattering spectra in a crystal containing a large number of volume defects.

Analysis of the spectra showed that ZrO_2–Y_2O_3 crystals possess directions of the exciting and scattered light for which the longitudinal acoustic phonons practically do not contribute to the *VV* spectra of the scattered light. This feature had been observed earlier in crystals of sapphire,[62] lithium niobate,[63,64] and solid solutions of HfO_2–Y_2O_3,[65] and recently also in a diamond crystal.[54] It has been attributed to mutual compensation between the pure-shear and uniform-compression deformations caused by the longitudinal (or quasi-longitudinal) sound wave and the changes in the dielectric constant that arise as the sound propagates.[62]

They found from the MB spectra of the ZrO_2–Y_2O_3 crystals the elastic and relative photoelastic constants. It turned out that these solid solutions show very strong anisotropy of the speed of sound.

Table III gives certain parameters of the ZrO_2–Y_2O_3 crystals.[61]

The intensity of the MB components declines linearly with decreasing temperature of the crystal. In the region of helium temperatures, it can become several orders of magnitude weaker than the undisplaced component, whose intensity is determined by crystal defects and does not depend on the temperature. Then the MB components can be simply submerged in the "tail" of the undisplaced component, as determined by the instrumental profile of the spectral instrument. An iodine light filter is also effective here for attenuating the undisplaced component.

TABLE III.

Y_2O_3 content mole%	ρ, g/cm³	Elastic anisotropy $\frac{C_{11}-C_{12}}{2C_{44}}$	n	Photoelastic constants P_{11}	P_{12}	P_{44} *)	Photoelastic anisotropy $\left\|\frac{P_{11}-P_{12}}{2P_{44}}\right\|$
10	5.95	2.40	2.193	—	—	—	1.80
12	5.89	2.56	2.183	−0.285	0.115	0.100	2.0
16.5	5.81	2.35	2.177	—	—	—	2.63
20	5.76	2.00	2.174	−0.470	0.101	0.100	2.85

*The constant P_{44} has been arbitrarily taken to be 0.100.

Studies were performed in[66] of MB light scattering in fused quartz and glasses in the temperature range 1.7–300 °K. The damping of the phonons in the studied temperature range was estimated experimentally. An I_2 filter was used to attenuate the stray light, which interfered with observing the MB components at low temperatures. An extra absorption line of iodine considerably attenuated the Stokes longitudinal (*L*) MB component, while the rest of the MB components (longitudinal and transverse) were distinctly observed in the scattered-light spectrum down to liquid-nitrogen temperatures. Only the *L* component was observed at 1.7 °K. The data of the measurements are collected in Table IV.

The free-flight paths of the phonons were calculated from the damping coefficient of sound, and the values were compared with those calculated from the thermal conductivity.

The iodine light filter as a spectrometer. Alekseev and Andreeva[67] have proposed using an absorbing cell, e.g., an iodine cell, to study narrow regions of a scat-

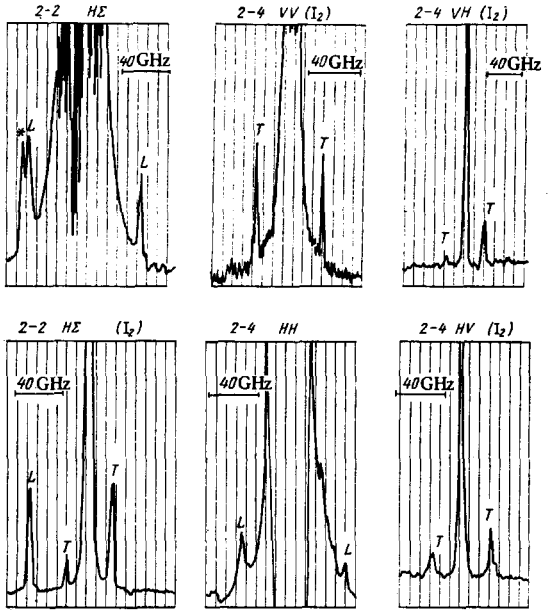

FIG. 25. Mandel'shtam-Brillouin spectrum in a cubic crystal of a solid solution of ZrO_2–Y_2O_3[61] (90 mole% ZrO_2, 10 mole% Y_2O_3). The designations of the spectra are as follows: the first symbol indicates the direction of propagation in the crystal of the incident light, and the second symbol that of the scattered light. 2—twofold axis, 4—fourfold axis. The polarizations of the incident and the scattered light are indicated by the letters *V*, *H*, and Σ. The first letter in order indicates the polarization direction of the incident light, and the second, the scattered light, *V* indicates the direction perpendicular to the plane of scattering, *H* parallel, and Σ indicates that no polarizer was used in the scattered light. I_2 indicates the use of an I_2 filter to attenuate stray scattered light.

TABLE IV.

Specimen	Component	Frequency, GHz	n	Speed of sound, km/sec	Damping coefficient, cm^{-1}
Fused quartz	L	23.5	1.462	5.85 ± 0.10	$> 2.0 \cdot 10^3$
	T	14.8		3.68 ± 0.10	$> 3.2 \cdot 10^3$
Borosilicate glass*	L	22.5	1.478	5.53 ± 0.07	$> 2.4 \cdot 10^3$
	T	14.0		3.45 ± 0.05	$> 3.8 \cdot 10^3$

*Composition of the glass: $SiO_2 \sim 80.5\%$, $B_2O_3 \sim 12.9\%$, $Na_2O \sim 3.8\%$, $Al_2O_3 \sim 2.2\%$, $K_2O \sim 0.4\%$, and $Li_2O \sim 0.2\%$.

tered-light spectrum. Their idea consists in the following: absorption is saturated in a cell containing a gas with intense coherent radiation of frequency ω_1 (nonlinear absorption), and a narrow transmission peak arises on the relatively broad Doppler absorption background $\Delta\omega_D$. The width of the transmission peak is of the order of the homogeneous width $\delta\omega$ of the absorption line. Scattered light that has been excited by radiation of frequency ω_0 is directed into this cell. Here the condition $|\omega_0 - \omega_1| \leq \Delta\omega_D$ must be satisfied. For the region of scattered-light frequencies $|\omega - \omega_1| \leq \delta\omega$, the light filter is more transparent than for other light frequencies. Therefore, by varying ω_1, we can record the intensity distribution of the overall contour (the convolution of the absorption line of iodine with the MB component). From the latter, we can isolate the intensity distribution in the scattered-light spectrum. This interesting proposal has not yet been realized experimentally.

They have proposed and carried out in[68] the use of an iodine light filter operating in a linear-absorption regime as a high-resolution spectrometer for studying narrow intervals of the spectrum (comparable with the width of the absorption line of iodine) near $\lambda = 5145$ Å.

The effectiveness of this spectrometer was demonstrated by studying the positions and widths of the Mandel'shtam-Brillouin (MB) components in four organic liquids.[68] This setup does not require using the interferometer as a spectral instrument. The principle of operation of this spectrometer is based on the idea that the absorption band of iodine vapor in the region of $\lambda = 5145$ Å is narrow, and it lies within the amplification band of the 5145 Å line of the stimulated emission of the Ar^+ laser (Fig. 26). One can select one longitudinal mode that is spectrally very narrow by introducing a Fabry-Perot etalon within the optical resonator of the laser. By varying the temperature of the etalon, and thus varying its optical length, one can pass from one mode to another by jumps whose size is determined by the dimensions of the optical resonator of the laser ($\Delta\nu = 1/2L$ cm^{-1}, where L is length of the optical resonator). Thus, by varying the frequency of the laser radiation, and passing it through an iodine cell, one can scan the absorption band of iodine by steps equal to $\Delta\nu$. This single-frequency radiation is so narrow that we can consider it to be a delta function, and therefore treat the obtained contour as being the true one.

If now we go from mode to mode by varying the temperature of the etalon, and illuminate the scattering volume (e.g., a liquid) with this light, while we direct the scattered light through an iodine cell into a photomultiplier, then the resultant curve will be the convolution of the contour of the absorption band of iodine I_2 and the region of the spectrum that corresponds, for example, to an anti-Stokes MB component (see Fig. 26). Then, for applying the iodine spectrometer, the scattering angle is chosen such that the frequency interval between the undisplaced and the MB components is narrower than that between the absorption line of iodine and the edge of the laser-action band of the Ar^+ laser, i.e., $f < \tilde{\nu} - \nu'$.

Since the shape of the absorption band of I_2 is known experimentally from scanning the absorption band of iodine, then in order to find the position of the maximum of the MB component and its half-width δ, we must know the relation between the intensity distribution as a function of frequency in the MB component and these quantities. This relationship is known.[1]

In[68], where they determined f and δ, they used an Ar^+ laser from the Coherent Radiation firm having $L = 1.15$ m and $\Delta\nu = 0.13$ GHz. The etalon that monochromated the radiation of the Ar^+ laser had a thickness of 1 cm, and its temperature was controled to an accuracy of ± 0.01 °C. The width of the laser-action band in the region of 5145 Å was about 8 GHz, and the width of the absorption band of iodine was 0.85 GHz. The width of the single-mode radiation of the laser was 0.04 GHz.

As a result, they got data from the convolution for the position f of the maximum and the width of the MB

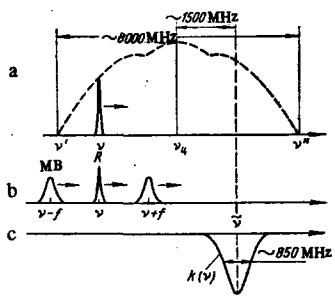

FIG. 26. Diagram explaining the use of an I_2 filter as a spectrometer, a) The output power of an Ar^+ laser as a function of the frequency of the axial mode for the 5145-Å line (weakly-marked magnetic Lamb dips can be seen); b) spectrum of the scattered light excited by a laser having the frequency ν (the Stokes and anti-Stokes and the Rayleigh components are indicated); c) position of the contour of the absorption line of the I_2 filter with respect to the laser-action line of the Ar^+ laser (ν is the center of the absorption line of iodine).

components. For carbon tetrachloride at the scattering angle $\theta = 63°52'$, $f = 3.088$, $\delta = 0.580$; in benzene at $\theta = 64°39'$, $f = 4.413$, $\delta = 0.34$; and in ethyl alcohol at $\theta = 61°50'$, $f = 3.100$, $\delta = 0.780$. The values of f and δ are given in GHz.

We note in conclusion that a combination of the iodine cell with a multipass Fabry-Perot interferometer has not yet been applied, yet quite evidently, such a combination could give very good results in studying narrow spectral intervals.

[1]I. L. Fabelinskiĭ, Molekulyarnoe rasseyanie sveta (Molecular Scattering of Light), Nauka, M., 1965 (Engl Transl., Plenum Press, New York, 1968).
[2]D. I. Mash, V. S. Starunov, and I. L. Fabelinskiĭ, Zh. Eksp. Teor. Fiz. 47, 783 (1964) [Sov. Phys. JETP 20, 523 (1965)].
[3]V. S. Starunov, I. L. Fabelinskiĭ, and E. V. Tiganov, Pis'ma Zh. Eksp. Teor. Fiz. 5, 317 (1967) [JETP Lett. 5, 260 (1967)].
[4]H. Z. Cummins, N. Knabe, and Y. Yeh, Phys. Rev. Lett. 12, 150 (1964).
[5]G. S. Landsberg and I. L. Mandel'shtam, Izbrannye trudy (Selected Works), Nauka, M., 1968, p. 103.
[6]H. Z. Cummins, in: Proc. of 2nd Intern. Conference on Light Scattering in Solids, Ed. M. Balkanski, Paris, Flammarion, 1971, p. 3.
[7]G. E. Devlin, J. L. Davis, L. Chase, and S. Geschwind, Appl. Phys. Lett. 19, 138 (1971).
[8]W. V. Houston, Phys. Rev. 29, 478 (1927).
[9]K. W. Meissner, JOSA 31, 405 (1941).
[10]C. Dufour, Ann. de Phys. 6, 5 (1951).
[11]J. R. Sandercock, Optics Comm. 2, 73 (1970).
[12]J. R. Sandercock, a) see Ref. 6, p. 9; b) RCA Rev. 36, 89 (1975).
[13]P. Jacquinot, Rep. Progr. Phys. 23, 267 (1960) [Usp. Fiz. Nauk 78, 123 (1962)].
[14]P. Connes, Rev. Opt. 35, 37 (1956); J. Phys. et Radium 19, 262 (1958).
[15]M. Hercher, Appl. Opt. 7, 951, 1336 (1968).
[16]A. G. Fox and T. Li, Bell Syst. Tech. J. 40, 453 (1961)].
[17]E. Gercke and A. E. Lau, Zs. Techn. Phys. 8, 157 (1927).
[18]P. Hariharan and A. D. Sen, JOSA 51, 398 (1961).
[19]J. R. Sandercock, Phys. Rev. Lett. 28, 237 (1972).
[20]D. S. Cannell, J. H. Lunacek, and S. B. Dubin, Rev. Sci. Instrum. 44, 1651 (1973).
[20a]D. Byesens, Rev. de Phys. Appl. 8, 175 (1973).
[21]D. S. Canell and G. B. Benedek, Phys. Rev. Lett. 25, 1157 (1970).
[22]J. H. R. Clarke, M. A. Norman, and F. L. Borsay, J. Phys. E8, 144 (1975).
[23]J. V. Ramsay, Optics Technology 1, 27 (1968).
[24]K. Mütze, L. Foitzik, W. Krgu, and G. Schreiber, Brockhaus ABC der Optik, Lpz., 1961, S. 902.
[25]R. E. Schoen and D. A. Jackson, J. Phys. E5, 519 (1972).
[26]W. L. Peticolas, G. W. Hibler, J. L. Lippert, A. Perterlin, and H. Olf, Appl. Phys. Lett. 18, 87 (1971).
[27]S. Esekiel and R. Weiss, Phys. Rev. Lett. 20, 91 (1968).
[28]J. P. Hohimr, R. C. Kelly, and P. K. Tittel, Appl. Opt. 11, 626 (1972).
[29]T. J. Ryan, D. G. Youmans, L. A. Hackel, and S. Esekiel, Appl. Phys. Lett. 21, 320 (1972).
[30]Yu. V. Troitskiĭ, Odnochastotnaya generatsiya v gazovykh lazerakh (Single-Frequency Laser Action in Gas Lasers), Nauka, Novosibirsk, 1975.
[31]I. L. Chistyĭ, V. F. Kitaeva, and N. N. Sobolev, IEEE J. Quantum Electron. QE-10, 38 (1974).
[32]I. L. Chistyĭ, V. F. Kitaeva, V. V. Osiko, N. N. Sobolev, B. I. Starikov, and M. I. Tomishechkin, Fiz. Tverd. Tela 17, 1434 (1975) [Sov. Phys. Solid State 17, 922 (1975)].
[33]N. A. Afonnikov, A. P. Boltaev, V. F. Kitaeva, A. E. Novik, V. P. Sasorov, and I. L. Chistyĭ, Zh. Prikl. Spektrosk. 11, 886 (1969).
[34]V. F. Kitaeva, N. N. Sobolev, I. P. Sisoz, Yu. V. Troitskiĭ, and I. L. Chistyĭ, in Kvantovaya élektronika (Quantum Electronics), No. 6, Sov. radio, M., 1971, p. 91 [Transl. by Plenum Press, p. 633].
[35]S. Itoh and T. Nakamura, Ferroelectrics 8, 589 (1974).
[36]S. Itoh and T. Nakamura, Japan J. Appl. Phys. Suppl. 14, 83 (1975).
[37]R. F. Elliot *et al.*, Proc. Roy. Soc. A328, 217 (1972).
[38]J. R. Sandercock, S. B. Palmer, R. J. Elliott, W. Hayes, Sr. P. Smith, and A. P. Young, J. Phys. C5, 3126 (1972).
[39]Y. Liao, N. A. Clark, and P. S. Pershan, Phys. Rev. Lett. 30, 639 (1973).
[40]R. K. Whener, Optics Comm. 6, 174 (1972).
[41]K. Vedam, W. Knausenberger, and F. Lukes, JOSA 59, 64 (1969). H. R. Philipp and E. A. Taft, Phys. Rev. 120, 37 (1960).
[42]W. C. Dash and R. Newman, *ibid.* 99, 1151 (1955).
[43]R. F. Potter, *ibid.* 150, 562 (1966).
[44]R. J. Archer, *ibid.*, 110, 354 (1958).
[45]a) G. Harbeke Zs. Naturforsch. 19a, 548 (1964). b) J. G. Dil and E. M. Brody, Rochester Univ. Preprint (N.Y.) 14627 (1975).
[46]J. R. Sandercock and W. Wettling, Sol. State Comm. 13, 1729 (1973).
[47]J. R. Sandercock, *ibid.* 15, 1715 (1974).
[48]A. I. Akhiezer, V. G. Bar'yakhter, and S. V. Peletminskiĭ, Spinovye volny (Spin Waves), Nauka, M., 1967 (Eng. Transl., North-Holland, Amsterdam, 1967).
[49]R. W. Dixon, J. Appl. Phys. 38, 3624 (1967).
[50]A. W. Smith, Phys. Rev. Lett. 20, 384 (1967).
[51]W. Wettling, M. G. Cottam, and J. R. Sandercock, J. Phys. C8, 211 (1975).
[52]J. R. Sandercock, Phys. Rev. Lett. 29, 1735 (1972).
[53]E. Brody, C. Roychoudhuri, and M. Hercher, Appl. Phys. Lett. 23, 543 (1973).
[54]M. H. Grimsditch and A. K. Ramdas, Phys. Lett. A48, 37 (1974); Phys. Rev. B11, 3139 (1975).
[55]J. Pelous and R. Vacher, Sol. State Comm. 16, 279 (1975).
[56]R. S. Krishnan, V. Chandrasekharan, and E. S. Rajagopal, Nature 182, 518 (1958).
[57]G. N. Ramachandran, Proc. Ind. Ac. Sci. A32, 171 (1950).
[58]F. Peter, Zs. Phys. 15, 358 (1923).
[59]W. L. Peticolas, G. W. Hibler, J. L. Lippert, A. Pertlin, and H. Olf, Appl. Phys. Lett. 18, 87 (1971).
[60]H. Rosen and Y. R. Schen, Mol. Cryst. and Liquid Cryst. 18, 285 (1972).
[61]V. I. Aleksandrov, V. F. Kitaeva, V. V. Osiko, N. N. Sobolev, V. M. Tatarintsev, and I. L. Chistyĭ, Kr. Soobshch. Fiz. (FIAN SSSR), No. 3, 27 (1975).
[62]I. L. Chistyĭ, V. F. Kitaeva, N. N. Sobolev, and V. P. Bakhar, Zh. Eksp. Teor. Fiz. 63, 1477 (1972) [Sov. Phys. JETP 36, 783 (1972)].
[63]D. F. Kiselev, T. M. Glushkova, and M. M. Firsova, Fiz. Tverd. Tela 11, 3592 (1969) [Sov. Phys. Solid State 11, 3007 (1970)].
[64]Z. M. Khashkhozhev, V. V. Lemanov, and R. V. Pisarev, Fiz. Tverd. Tela 12, 128 (1970) [Sov. Phys. Solid State 12, 101 (1970)].
[65]V. I. Aleksandrov, V. F. Kitaeva, I. V. Kolzov, V. V. Osiko, N. N. Sobolev, V. M. Tatarintsev, and I. L. Chistyĭ, Kristallografiya 17, 1085 (1973) [Sov. Phys. Crystallogr. 17, 968 (1974)].
[67]V. A. Alekseev and T. L. Andreeva, Pis'ma Zh. Eksp. Teor. Fiz. 20, 316 (1974) [JETP Lett. 20, 140 (1974)].

Translated by M. V. King